Dalton Transactions

ROYAL SOCIETY OF CHEMISTRY

PAPER

View Article Online
View Journal | View Issue

Check for updates

Cite this: *Dalton Trans.*, 2025, **54**, 8270

Platinum(II) and ruthenium(II) coordination complexes equipped with an anchoring site for binding the protein kinase enzyme pockets: synthesis, molecular docking and biological assays†‡

Matthieu Scarpi-Luttenauer,[a] Katia Galentino,[b] Christophe Orvain, §[c] Audrey Fluck, [a] Marco Cecchini, [b] Georg Mellitzer,§[c] Christian Gaiddon *¶[c] and Pierre Mobian *[a]

Received 25th October 2024,
Accepted 10th December 2024

DOI: 10.1039/d4dt02984d

rsc.li/dalton

To mimic the structural aspects of staurosporine, a potent but unspecific kinase inhibitor, several coordination compounds based on two readily available diimine ligands containing hydrogen bonding donor/acceptor sites (NH–CO fragment) have been designed and synthesized. These complexes are constructed around Ru(II) and Pt(II) metal centers. A total of 9 compounds, named **Ru(1)–(5)** and **Pt(1)–(4)**, were obtained through straightforward synthetic approaches. The cytotoxicity of the compounds was evaluated on AGS gastric cancer cells (GC) through standard MTT assays. All ruthenium and platinum complexes with low toxicity, *i.e.* **Ru(3)**, **Ru(5)**, **Pt(3)** and **Pt(4)**, were docked in the ATP binding pocket of two protein kinases (S6K1 and MST2). The docking scores highlighted a preferred affinity of **Ru(5)** for the MST2 binding pocket, whereas the platinum compounds are predicted to bind stronger to the S6K1 binding site. Inhibitory activity of the metal complexes on the MST2 and S6K1 signaling pathways was evaluated by analyzing *via* western blot experiments the phosphorylation state of YAP, a downstream component of the Hippo pathway and the protein expression of S6 and its phosphorylated analogue p-S6. A clear difference of behavior between the Pt(II) and the Ru(II) complexes depending on the type of kinase was observed.

Introduction

Protein kinases are an essential class of enzymes which play a fundamental role in human cellular signaling pathways.[1] These enzymes are crucial for the regulation of cellular metabolism, including cell growth and survival. They catalyze the addition of a phosphate group originated from the hydrolysis of ATP onto a target substrate, such as a protein, a sugar or a lipid. In some cases, overexpression or mutations in protein kinases can contribute to tumor growth.[2–7] Hence, protein kinase inhibitors represent a promising class of anticancer drugs allowing the selective inhibition of a protein kinase involved in cancer development or spreading. In addition, these inhibitors are essential tools to understand the role of kinases in signaling pathways and physio-pathological processes. Currently, 80 different protein kinase inhibitors are already used for the clinical treatment of different cancer types.[8] Most of them are organic compounds built around a long organic scaffold containing hydrogen-bond donor and acceptor sites for efficient binding of the drug into the ATP binding pocket of the enzyme. Thus, the interaction between the drug and the enzyme hinders the interaction of the latter with ATP. Since the structure of the ATP binding pocket of all protein kinases is highly conserved, it is a challenging task to engineer selective inhibitors.

Staurosporine is a natural alkaloid acting as an extremely potent protein kinase inhibitor (Fig. 1).[9–11] The structure of this molecule is composed of a flat indolocarbazole fragment responsible for the binding to the active site of the enzyme

---

[a] *Université de Strasbourg, CNRS, UMR 7140, F-67000 Strasbourg, France. E-mail: mobian@unistra.fr*
[b] *Université de Strasbourg, CNRS, UMR 7177, F-67000 Strasbourg, France*
[c] *Inserm U1113 IRFAC, Team STREINTH, Strasbourg, France*

† This article is dedicated to the memory of Pr. Marc Henry.

‡ Electronic supplementary information (ESI) available. CCDC 2392833 and 2392834. For ESI and crystallographic data in CIF or other electronic format see DOI: https://doi.org/10.1039/d4dt02984d

§ Present address: INSERM, UMR 1260, CRBS, Regenerative Nanomedicine, "GP_SMIT" Laboratory, CRBS; 1 Rue Eugène Boeckel, 67085 Strasbourg, France.

¶ Present address: UMR7242, Biotechnology et Signalisation Cellulaire, group STREINTH, 300 Bld S. Brant, FR-67412 Illkirch Cedex, France.

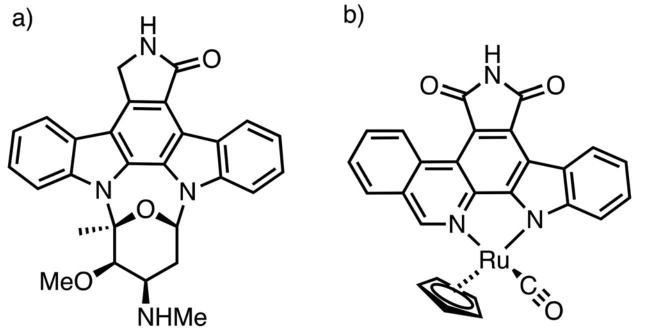

Fig. 1 (a) Staurosporine; (b) an example of an organometallic Ru(II)-complex mimicking the structural aspects of staurosporine developed by Meggers *et al.* as inhibitor of the MST1 kinase.

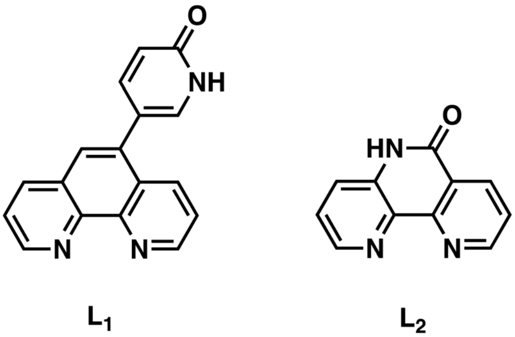

Fig. 2 Ligands L_1 and L_2.

through hydrogen bonding interactions and a voluminous glycosidic unit. While being extremely potent, staurosporine is not selective, which prevented its use in clinical studies.

Despite this lack of selectivity, the structure of this efficient kinase inhibitor has inspired the design of non-natural kinase inhibitors. In this context, Meggers *et al.* have developed metal complexes mimicking the structural aspects of staurosporine to prepare kinase inhibitors incorporating a metallic scaffold. Starting from a sophisticated pyridocarbazole-based bidentate nitrogen ligand, they were able to vary the coordination sphere around the metal for fine-tuning selectivity of the inhibitors, yielding a library of different metal complexes, exhibiting nM-range, *in vitro* IC_{50} towards different protein kinases with a very high selectivity.[12–15] In particular, Meggers *et al.* identified inhibitors for MST1 (see Fig. 1b). MST1 is a kinase involved in the Hippo pathway that plays a critical role in mecanotransduction (regulation of cell and organ growth *via* physical force sensing) and proliferation/survival *via* the transcription cofactors YAP and TAZ.[16,17] Alterations of this pathway leads to cancer progression by hyperactivation of YAP and/or TAZ. Inspired by the Meggers lab strategy, we have tried to develop novels and more selective inhibitors for MST1/2 kinases.

Recently, we have reported octahedral titanium(IV) complexes constructed around a TiO_4N_2 core where the nitrogen bidentate ligands linked to the metal center bear hydrogen bond donor and acceptor recognition units (NH–C=O). Docking experiments with these titanium complexes on the Hippo protein kinase MST2 showed that the titanium complexes were too voluminous to fit the binding site of the kinase. Nevertheless, the free ligands, compounds L_{1-2} (Fig. 2), fitted well the enzymatic pocket of this kinase.[18] The phenanthroline ligand L_1 functionalized with a pyridinone unit at the position 5, and the diimine ligand L_2, on which two pyridine moieties are fused together by an amide group are easily accessible in a few synthetic steps. Hence, these two ligands represent good candidates to mimic the flat indolocarbazole fragment found in staurosporine.[18,19] Thus, L_{1-2} appeared as two interesting building starting units to develop metal complexes having an optimized shape regarding the enzyme binding pocket of MST2. In addition, compounds L_{1-2} showed good solubility in organic media allowing their facile use for the preparation of various transition metal complexes.

Here, we report the synthesis of transition metal complexes bearing the L_{1-2} diimine ligands. For this purpose, Ru(II) and Pt(II) were selected to generate species offering distinct geometries. Moreover, they are thoroughly investigated in therapeutic chemistry devoted to anticancer treatments. Development of novels Ru(II) and Pt(II) complexes may provide solutions to avoid the existing resistance mechanisms.[20–25] Ru(II) typically displays octahedral or pseudo-octahedral coordination spheres, whereas 4-fold coordinated Pt(II) compounds adopt a square planar geometry. In addition, the carbon ruthenium bond in Ru(II) complexes confers original biological activities linked to the redox behavior of these organometallic species.[26]

Hence, we have prepared several Ru(II) or Pt(II) complexes based on ligand L_1 or L_2 displaying a diversity of shapes and geometries aiming at characterizing their potential to inhibit enzymatic activities, in particular MST1/2. The cytotoxicity of these complexes was then assayed, followed by structure–activity relationship evaluation *via* molecular docking in a protein kinase of the Hippo pathway, MST2. To compare the selectivity, we extended the structure–activity studies to S6K1, which is a key regulatory enzyme of the activity of the ribosomal protein S6. The docking predictions were validated experimentally with the quantification of the phosphorylation of YAP, the downstream component of the Hippo pathway,[27] and S6, the phosphorylation target of S6K1.[28]

Results and discussion

Synthesis of Pt(1)–(4) and Ru(1)–(5) complexes and hydrolytic stability

Aiming to develop new coordination compounds mimicking the structural aspects of the staurosporine, we have prepared a series of ruthenium(II) and platinum(II) complexes incorporating the ligands L_1 or L_2. The synthetized complexes are depicted in Fig. 3.

A total of 5 ruthenium(II) complexes were synthetized from either ligand L_1 or L_2. The synthetic protocols allowing the preparation of these complexes are given in Fig. 4. The synthesis of octahedral ruthenium(II) polypyridyl complexes **Ru(1)** and **Ru(2)** was first carried out starting from known dichloro

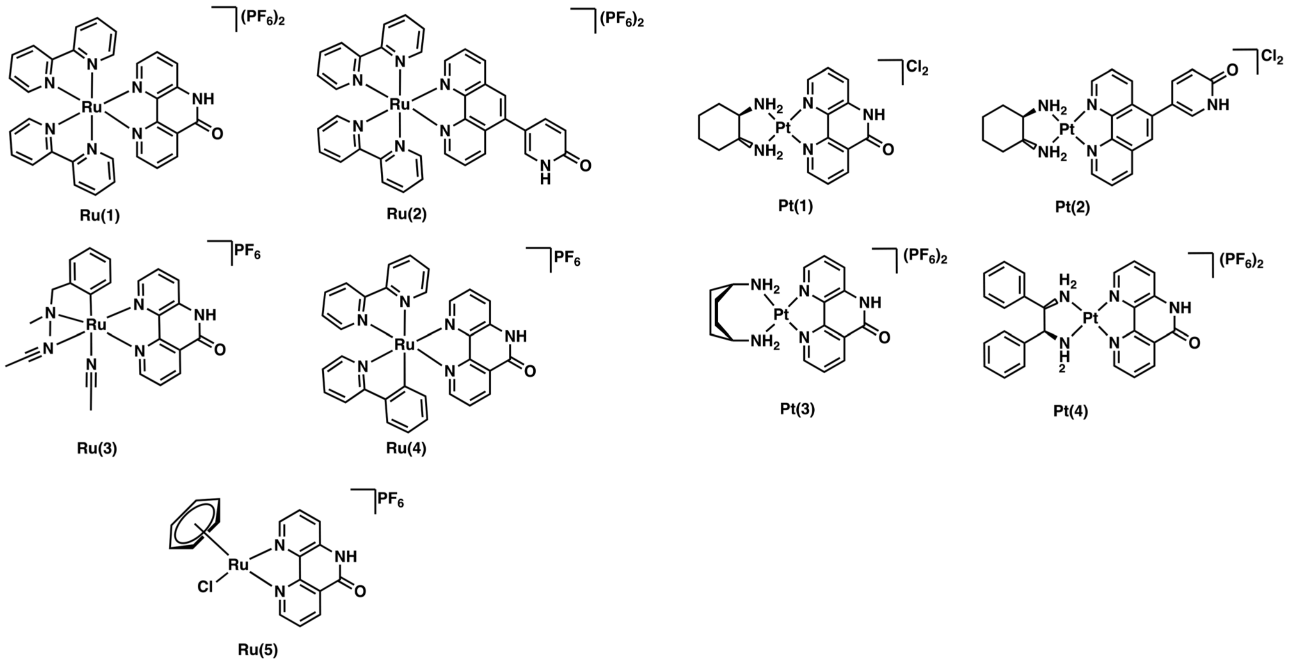

Fig. 3 Pt(II) and Ru(II) complexes studied in this work.

precursor [Ru(bpy)$_2$Cl$_2$] (**1**) which reacted with ligands **L_1** and **L_2** respectively in an ethylene glycol/water 90 : 10 mixture for 6 hours as detailed in Fig. 4.[29] After precipitation with the addition of a saturated aqueous KPF$_6$ solution, purification by column chromatography of the crude products over silica gel resulted in the isolation of **Ru(1)** and **Ru(2)**.

The two complexes were characterized by ^{1}H and ^{13}C NMR spectroscopy, ESI-MS and elemental analysis. Single crystals of **Ru(2)** were obtained when diethyl ether vapors were allowed to diffuse in an acetone solution of the complex. The solid-state structure of **Ru(2)** resolved by single crystal X-Ray diffraction is shown in Fig. 5.

The compound **Ru(2)** displays a slightly distorted octahedral geometry. The N–Ru–N angles between the nitrogen atoms in *trans* are of 172.3°, 173.6° and 173.7°. The N–Ru bond lengths between the bipyridine ligands and the metal are comprised between 2.061 and 2.071 Å, whereas the N–Ru bond lengths between the ligand **L_2** and the metal are slightly longer (2.076 Å and 2.078 Å). The N–Ru–N angles displayed by the two bipyridine ligands are similar (78.6° and 78.7°), whereas the one displayed by **L_2** is slightly wider (79.7°). Surprisingly, the solid-state arrangement of **Ru(2)** shows that the amide fragment of **L_2** is involved in a hydrogen bond interaction with the oxygen atom of an acetone molecule, which is characterized by a $\underline{N}$–H⋯$\underline{O}$ length of 2.840 Å (Fig. 5b) which contrasts with the dimerization observed for the previous reported Ti(IV)-complex bearing the same nitrogen ligand L_2.[16]

Cycloruthenated complexes **Ru(3)** and **Ru(4)** were prepared by adapting procedures described by Pfeffer *et al.*[30,31] **Ru(3)** was prepared by reacting precursor **2** with ligand **L_2** at 45 °C for 3 days. After purification by column chromatography over silica gel, the desired compound was obtained in a moderate yield of 20%. The ^{1}H NMR spectrum of **Ru(3)** is complex due to the dissymmetry of the ligand **L_2**. The ^{1}H NMR spectrum of **Ru(3)** displays 20 signals which were attributed according 2D ^{1}H and ^{13}C NMR analysis to the two different isomers shown Fig. 6a. In particular, the 2D ROESY spectrum proved the presence of these two isomers since two demonstrative correlations are observed as shown in Fig. 6b. The first correlation was found between the H_9 proton belonging to **L_2** and the benzylamine H_a proton of one stereoisomer. The second correlation was assigned to the **L_2** $H_{2'}$ proton and the benzylamine $H_{a'}$ proton of the second stereoisomer. This unique spatial proximity between the benzylamine proton and one **L_2** proton ($H_{2'}$ or H_9) per isomer was verified by constructing molecular models of each isomer and analyzing the crystal structure of an analogous complex where the ligand **L_2** is replaced by a 2,2′-bipyridine ligand.[32] DOSY NMR analysis confirmed that the two species were stereoisomers as only one diffusion value of $D = 7.00 \times 10^{-10}$ m^2 s^{-1} was obtained. Additionally, integration of the signals on the ^{1}H NMR spectrum revealed that the two stereoisomers are found in a 1 : 1 ratio in solution.

Ru(4) was synthesized by reacting **L_2** with precursor **3**[33] in methanol at reflux overnight. The desired complex was isolated by column chromatography over alumina. NMR analysis of the compound showed a similar situation as described for **Ru(3)**, as the spectrum showed more signals related to the presence of a single stereoisomer in solution as two sets of signals are observed by ^{1}H NMR. Furthermore, the 2D COSY spectrum allowed the identification of the signals for **L_2** for each stereoisomer. Additionally, **Ru(3)** and **Ru(4)** were also characterized by ESI-MS and elemental analysis.

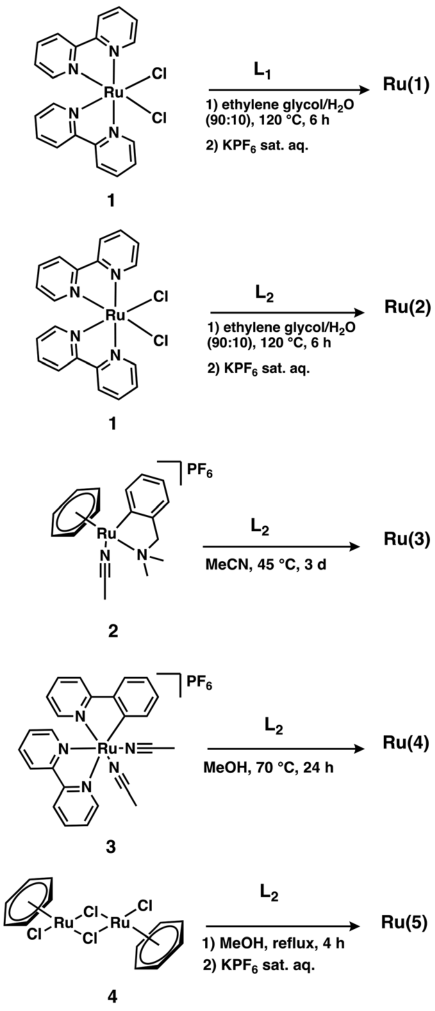

Fig. 4 Synthetic pathways leading of complexes **Ru(1)**–**(5)**.

Piano-stool complex, **Ru(5)**, was synthesized according to a procedure described by Queyriaux *et al.*[34] The one-step reaction of commercially available dimeric species **4** with $\mathbf{L_2}$ in methanol at reflux during 4 h allowed after precipitation with saturated aqueous KPF_6 the isolation of the desired complex which was characterized by ^{1}H and ^{13}C NMR spectroscopy, ESI-MS spectrometry and elemental analysis.

The synthetic pathways leading to the formation of square-planar Pt(II) complexes containing either ligand $\mathbf{L_1}$ or $\mathbf{L_2}$ are described in Fig. 7. Robust square-planar PtN_4 complexes incorporating diimine ligands for DNA intercalation have recently been described by Aldrich-Wright *et al.*[35–37] This scaffold appeared of great interest for the synthesis of protein kinase inhibitors constructed around a square-planar Pt(II) core incorporating ligands $\mathbf{L_1}$ and $\mathbf{L_2}$ (Fig. 7).

Pt(1) and **Pt(2)** were prepared by reacting known 1,2-diaminocyclohexane (1,2-DACH) precursor **[Pt(1,2-DACH)Cl₂]** (**5**) with ligands $\mathbf{L_1}$ and $\mathbf{L_2}$ respectively in water at reflux.[35] The desired complexes were then isolated after purification over reverse phase resin.

Pt(3) was synthesized in a one-pot two steps procedure.[36] First, the chloro ligands were eliminated with the addition of $AgNO_3$ to the kiteplatin precursor **6** in DMF. In a second step, the AgCl precipitate was centrifuged, and $\mathbf{L_2}$ was added to the supernatant. The resulting mixture was stirred first at room temperature for 16 hours and next at 50 °C for one day. The desired complex **Pt(3)** was isolated after purification over reverse phase resin.

Finally, complex **Pt(4a)** incorporating (*S*,*S*)-diphenylethylenediamine (**9**) was prepared in a two-step procedure. First, the dichloro precursor **8** was obtained from the substitution of the DMSO ligands of **[Pt(DMSO)₂Cl₂]** (**7**) by $\mathbf{L_2}$.[37] The complex was then refluxed without further purification with the corresponding nitrogenated ligands to yield the targeted complex. The solid-state structure of **Pt(4)** obtained after single crystal XRD analysis is shown in Fig. 8a. The crystalline packing

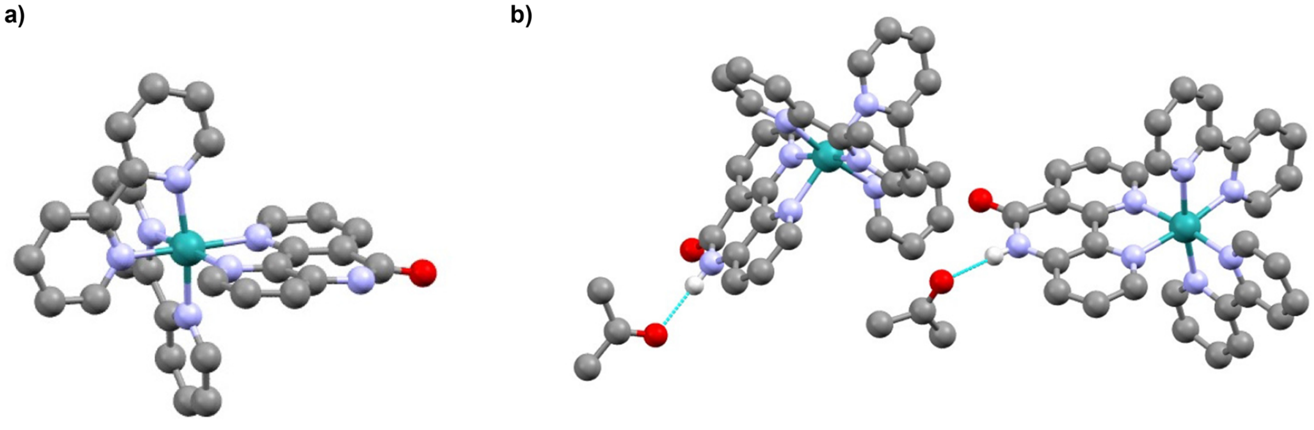

Fig. 5 (a) Ball and stick representation of the solid-state structure of **Ru(2)**, obtained from single-crystal X-ray crystallography (CCDC 2392833‡). (b) **Ru(2)** packing in the crystal. The hydrogen bonds are represented in blue. Ruthenium atoms are depicted in turquoise, oxygen atoms in red, carbon atoms in grey, nitrogen atoms in blue and hydrogen atoms in light grey. The hydrogen atoms, the PF_6^- anions and the acetone crystallization solvent molecules are omitted for clarity.

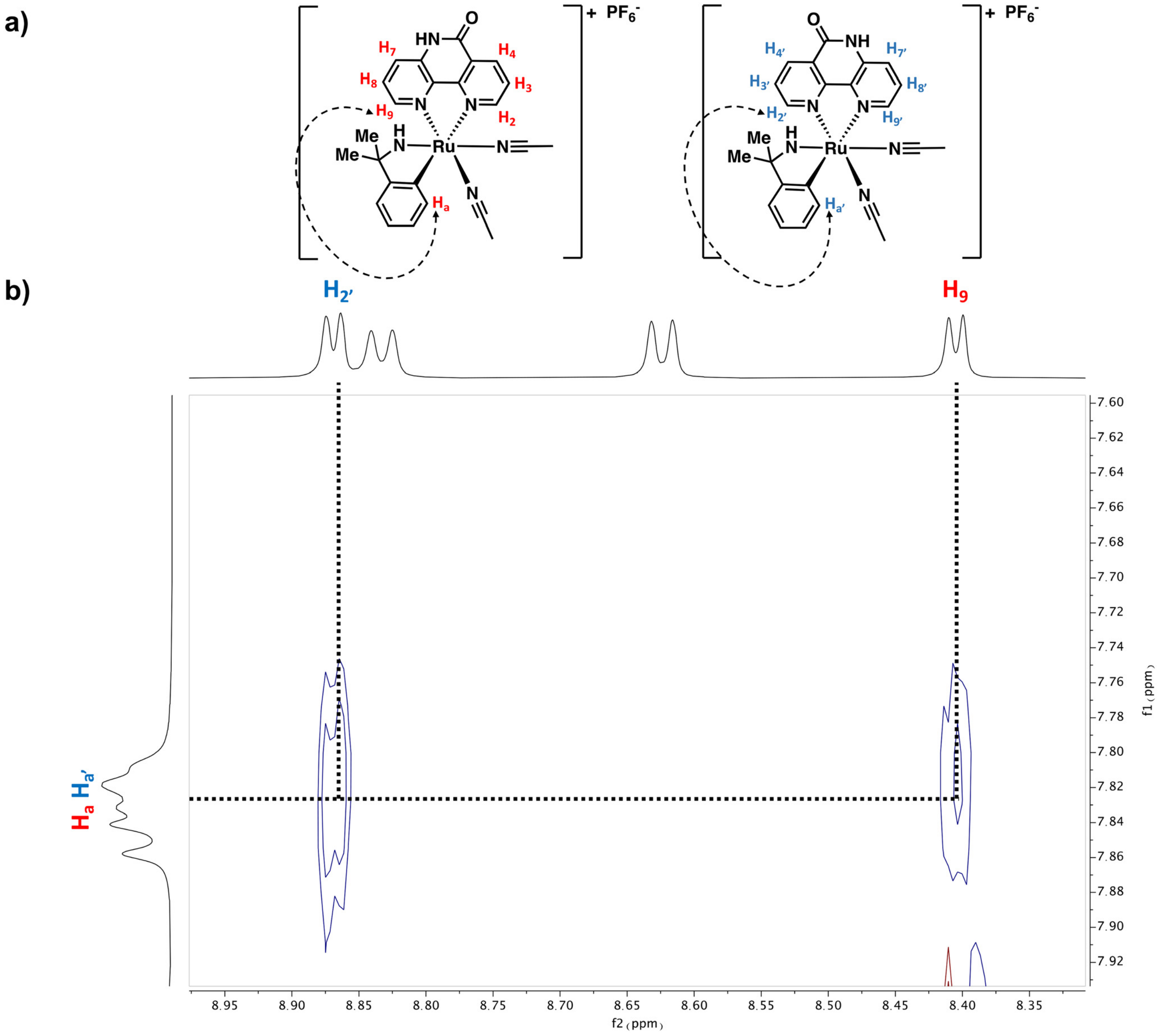

Fig. 6 (a) Representation of the two stereoisomers corresponding to **Ru(3)**. The arrows indicate the correlation in space between the two protons seen on the ROESY spectrum, for each isomer. (b) Region of the 2D ROESY spectra of **Ru(3)** highlighting two strong correlations; one between the protons $H_{a'}$ and $H_{2'}$ and a second between H_a and H_2.

shows that the complex units are stacked together through the diimine ligand (Fig. 8b). The mean distance between the closest carbon atoms is of 3.424 ± 0.049 Å. Surprisingly, in the crystal, the amide fragments of ligand $\mathbf{L_2}$ are deprotonated, which leads to hydrogen bonding interactions ($N(\mathbf{L_2})\cdots HN(\mathbf{9})$) between this deprotonated nitrogen and NH_2 proton of the diamino ligand **9** (N⋯HN length = 3.222 Å).

In order to evaluate the hydrolytic stability of the **Ru(1)–(5)** and **Pt(1)–(4)** complexes, the evolution of UV-visible absorption spectra of these complexes were recorded in Phosphate Buffer Saline (PBS). Stock solutions of the complexes in DMSO (c = 50 mM) were diluted in an aqueous PBS buffer solution to reach a concentration of c = 50 μM and a spectrum was recorded every hour. A slight drop in intensity was observed for the analyzed complexes, which was explained by the medium evaporation (see the ESI‡).

Overall, no changes were noticed, meaning that the complexes are stable in a biologically relevant condition. The only exception concerned complex **Ru(3)**. The recorded spectra are displayed Fig. 9. Over time, a hypsochromic shift of the visible absorption band was observed with an isosbestic point at λ = 455 nm. This observation indicated that the initial complex **Ru(3)** was slowly converted into a new species. Since Pfeffer *et al.* have previously demonstrated that the acetonitrile ligands within analogous complexes can be substituted by water molecules, it was assumed that the observed transformation for **Ru**

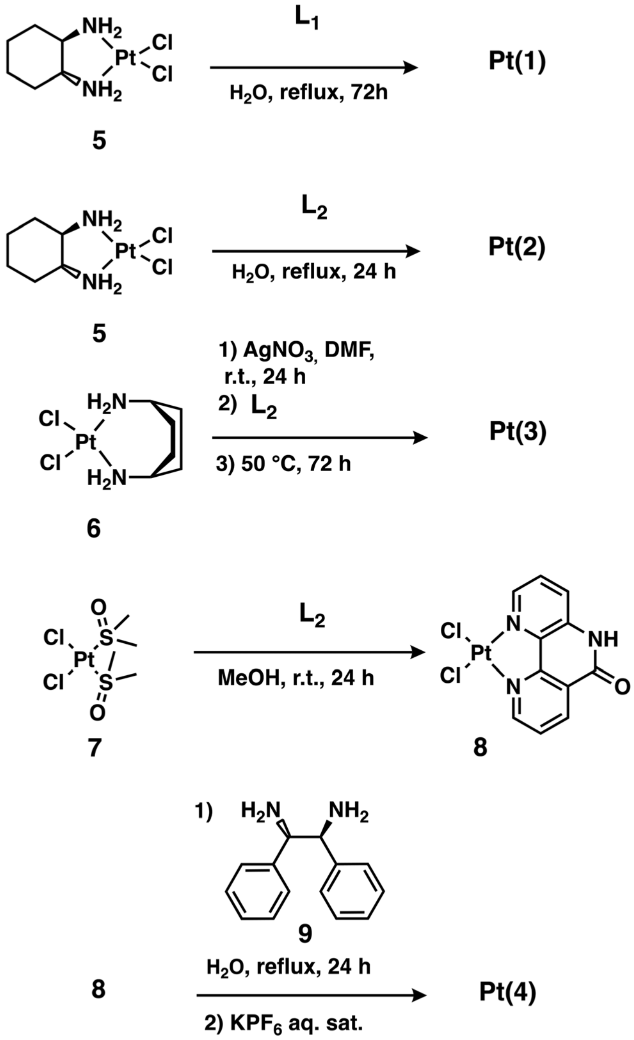

Fig. 7 Synthetic pathways leading to complexes **Pt(1)–(4)**.

(3) was linked to ligands exchange.[38] To confirm this hypothesis, the solution of **Ru**(3) in PBS obtained after 24 hours was analyzed by HPLC-MS.

Table 1 summarizes the major signals observed, and the *m*/*z* values associated with them. An adduct corresponding to the product on which one acetonitrile ligand has been exchanged by a DMSO molecule can be found at 3.87 min, meaning that the acetonitrile ligands have already been exchanged in the stock solution in DMSO. Finally, the evolution of a **Ru**(3) solution in CD_2Cl_2 in which D_2O (50 µL) were added was monitored by ^{1}H NMR analysis. Fig. 10 highlights the presence of an increasing amount of free acetonitrile at 1.97 ppm over time (24 h). After 48 h, the presence of free CH_3CN is even accentuated. Altogether, these analysis indicated that the acetonitrile ligands are labile ligands within **Ru** (3) and can be substituted by coordinating species such as DMSO or water.

Overall, several Ru(II) and Pt(II) complexes bearing either ligand $\mathbf{L_1}$ or $\mathbf{L_2}$ were synthetized using straightforward approaches. These species were fully characterized and their stability in a medium compatible with the biological assays evaluated. We noticed that **Ru**(3) was unstable under these conditions due to the substitution of labile acetonitrile ligands. Nevertheless, after this ligand exchange, the rest of the **Ru**(3) backbone remained unaltered.

In vitro cytotoxic activity of the Ru(II) and Pt(II) complexes

Having in hands this series of metal complexes designed for kinase inhibition, the impact of the Ru(II) and Pt(II) complexes on cell survival was evaluated. For instance, inhibition of MST1/2 should favors YAP/TAZ function, leading to increase survival and proliferation. Thus, the cytotoxicity of the compounds was evaluated through standard MTT assays. We choose the AGS GC cells as GC is a particularly aggressive cancer with limited therapeutic options that has been shown

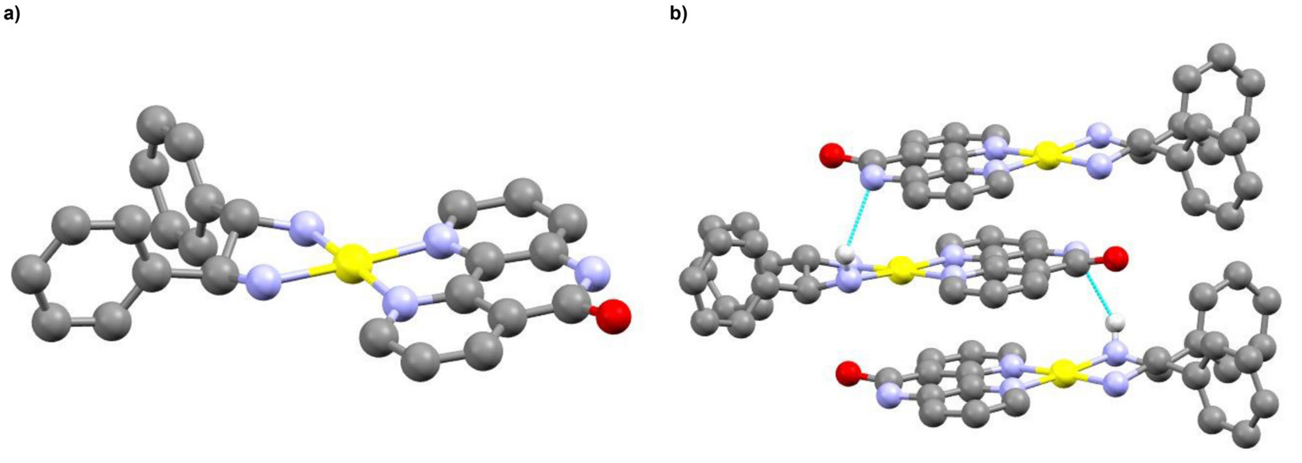

Fig. 8 (a) Ball and stick representation of the solid-state structure of **Pt(4)**, obtained from single-crystal X-ray crystallography (CCDC 2392834‡). (b) **Pt(4)** packing in the crystal. The hydrogen bonds are represented in blue. Platinum atoms are depicted in yellow, oxygen atoms in red, carbon atoms in grey, nitrogen atoms in blue and hydrogen atoms in light grey. The hydrogen atoms (excepted the H atoms involved in the hydrogen bonding), the PF_6^- anion and the DMF crystallization solvent molecules are omitted for clarity.

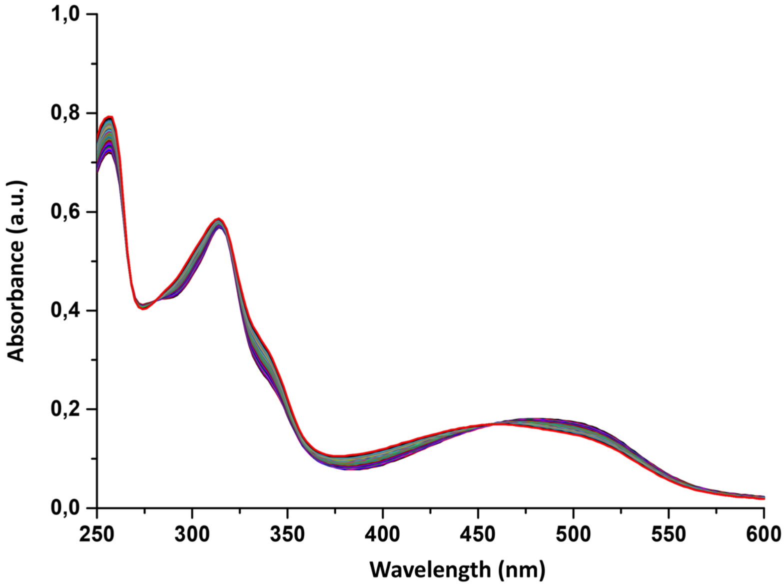

Fig. 9 UV-visible hydrolytic stability assay for **Ru(3)** in PBS buffer (c = 50 μM). A spectrum was recorded every hour over 24 h.

Table 1 Main HPLC signals and adducts observed from the analysis of a solution of **Ru(3)** after 24 h

Retention time (min)	m/z (z)	Adduct
3.16	217.0335 (2)	$[C_{20}H_{20}N_4ORu + H]^{2+}$
	258.0600 (2)	$[C_{24}H_{25}N_6ORu + H]^{2+}$
3.87	552.1039 (1)	$[C_{24}H_{28}N_5O_2RuS]^+$
4.15	515.1166 (1)	$[C_{24}H_{26}N_6ORu]^+$

to have deregulation in the YAP/TAZ pathway.[39] The Ru(II) and Pt(II) complexes and oxaliplatin (oxa), reference chemotherapy for the treatment of gastric cancer patients,[40] were incubated for 48 h with AGS cells. Cell viability was then determined by addition of MTT and absorption measurements and IC_{50} values were calculated (Table 2).

Ru(1) to **Ru(3)** and **Ru(5)** are considered with a very low or moderate toxicity since their IC_{50} values are over 100 μM.

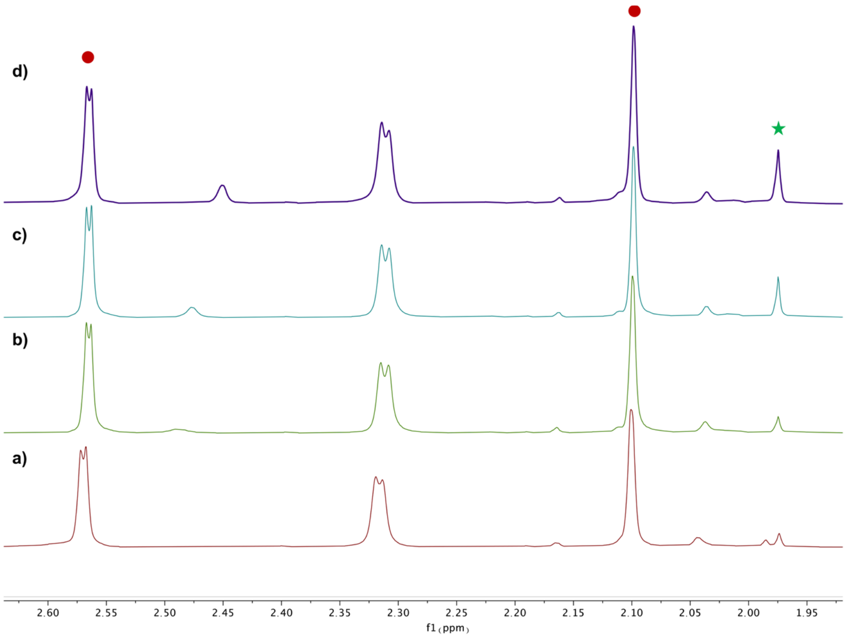

Fig. 10 Close-up on the acetonitrile CH_3 protons from the ^1H NMR spectrum of **Ru(3)** in a mixture $CD_2Cl_2 : D_2O$ 8 : 1. The coordinated acetonitrile signals are labelled by a red dot and the free acetonitrile signals are signaled by a green star. The spectra were recorded: (a) before the addition of D_2O, (b) just after the addition of D_2O, (c) 24 h after the addition of D_2O and (d) 48 h after the addition of D_2O.

Table 2 IC_{50} values ± SEM of oxaliplatin (Oxa) the Ru(II) and Pt(II) complexes tested towards AGS cells for 48 h

	IC_{50} (μM)
Ru(1)	104 ± 23
Ru(2)	164 ± 27
Ru(3)	>200
Ru(4)	13 ± 2.0
Ru(5)	>200
Pt(1)	16 ± 3.5
Pt(2)	5.5 ± 2.6
Pt(3)	>200
Pt(4)	>200
Oxa	1.7 ± 0.8

Despite being really close to **Ru(1)** from a structural view point, complex **Ru(4)** exhibited a much lower IC_{50} (13 ± 2.0 μM). The cytotoxic properties of **Ru(4)** analogues were studied by Pfeffer *et al.*[41] They reported that the cytotoxicity of these cyclometallated Ru-complexes arise from the redox properties of such complexes containing a Ru–C linkage. Hence, the toxicity displayed by **Ru(4)** is assumed to be a consequence of the Ru–C bond within this species.

Concerning the Pt(II) species, only **Pt(1)** and **Pt(2)** showed cytotoxicity when incubated with AGS cells (IC_{50} = 16 ± 3.5 and 5.5 ± 2.6 μM respectively). The biological activity of similar analogues was first reported by Aldrich-Wright *et al.*[42] The cytotoxic effect of these complexes were attributed to their capacity to intercalate double-stranded DNA, due to their planar structure. Therefore, it is not surprising to see that **Pt(3)** and **Pt(4)**, bearing more bulky 1,4-DACH or diphenylethylenediamine ligands, respectively, were non-toxic.

Docking studies of the Ru(II) and Pt(II) complexes in MST2 and S6K1

Based on the cytotoxicity of the synthesized complexes, only the compounds with low toxicity (IC_{50} > 200 μM) were selected for docking studies on two protein kinases, *i.e.* S6K1 (4rlp.pdb) and MST2 (5dh3.pdb). These proteins have two distinct cellular functions. MST2 is part of the Hippo signaling pathway, which contributes to the regulation of organ growth and apoptosis activation,[16] and is a relevant target for studying the effects of downregulation of the Hippo pathway on cellular growth.[17] S6K1 is a protein kinase that controls the activity of the 40S ribosomal protein S6 promoting protein synthesis.[43] Both the 40S ribosomal protein S6 and S6K1 have been implicated in morbidity such as diabetes, aging, obesity or even cancer.[44–46]

Eight docking experiments were carried out using the software PLANTS with the CHEMPLP scoring function,[47] which includes energy contributions accounting for hydrogen bonding, protein–ligand shape complementarity, and intraligand torsion and clash penalties (see Methods for details). To validate the docking protocol, we re-docked the two ligands co-crystallized with the MST2 and S6K1 kinases and compared results with the X-ray structures. The RMSD between the predicted lowest-energy binding pose and the experimentally determined X-ray binding pose was 0.5 Å for XMU-MP-1 in MST2[17] and 0.89 Å for FL772 in S6K1.[48] The re-docked compounds show significant overlap with the crystal coordinates establishing the same interactions with the protein (see ESI, Fig. S31‡).

All non-toxic ruthenium and platinum complexes, *i.e.* **Ru(3)**, **Ru(5)**, **Pt(3)** and **Pt(4)**, were docked in the ATP binding pocket of the two protein kinases. The docking results indicate a different propensity of the ligands to bind S6K1 or MST2 and predict that the platinum compounds **Pt(3)** and **Pt(4)** have a better docking score for S6K1, whereas the ruthenium compound **Ru(5)** interacts stronger with MST2 (Table 3). Concerning **Ru(3)**, the docking calculations predict an unfavorable interaction at MST2 likely due to steric clashes with the protein, as indicated by the positive score in Table 3.

Fig. 11 shows an overview of the key protein–ligand interactions that each compound establishes in the binding site of the kinase for which it has the best docking score. Analysis of the protein–ligand interactions using the software PLIP[49] provides insights into the binding selectivity. The comparison with the interaction patterns established by the reference compounds in the X-ray structures (*i.e.* FL772 in S6K1 and XMU-MP-1 in MST2) reveals that the ruthenium compounds fit reasonably well the ATP-binding pocket at S6K1 but they are unable to establish the critical H-bonds that steer protein–ligand recognition likely due to their shape or bulkiness of the substituents (Table S1‡). By contrast, the platinum compounds show a suboptimal fit of the ATP-binding pocket in MST2 albeit establishing similar hydrogen bonding interactions as the reference compound (Table S2‡). We conclude that the binding selectivity predicted by docking originates from an interplay of shape complementarity and directional interactions steering the recognition of rigid and bulky ligands at the nucleotide binding site of the two kinases.

Inhibitory activity of the metal complexes in MST2 and S6K1

Having docked both Ru(II) and Pt(II) complexes in MST2 and S6K1, we next aimed to evaluate their inhibitory activity *in vitro* using the GC cell line AGS. GC is a public health problem due to high aggressiveness with a 5-year survival rate of less than 25% and a median survival of about 11 months.[50] The reasons for this high mortality are multiple, including the variability in

Table 3 Docking results. The first column lists the 4 compounds that were tested *in vitro* (see below). The second and third columns report the docking score of the best binding pose per compound in S6K1 and MST2, respectively. In the last column, the difference between the docking scores is given

Compound	4rlp (S6K1)	5dh3 (MST2)	Δ(S6K1-MST2)
Ru(3)	−61.3	+13.7	−75
Ru(3)–H_2O	—	−57.8	—
Ru(3)–DMSO	—	+12.7	—
Ru(5)	−68.9	−74.6	+5.7
Pt(3)	−79.5	−67.5	−11.9
Pt(4)	−91.5	−68.6	−22.8

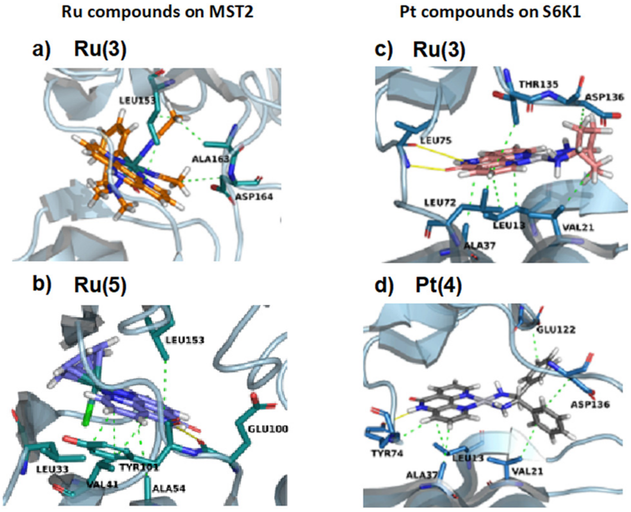

Fig. 11 Protein–ligand interaction profiles of **Ru(3)** and **Ru(5)** compounds in MST2 (PDB code: 5dh3) and of **Pt(3)** and **Pt(4)** compounds in S6K1 (PDB code: 4rlp). Hydrogen bonding and hydrophobic interactions are highlighted in yellow and green, respectively.

response to first treatment at equivalent tumor stage and that about 75% of cancers become resistant. Patient management is still based on surgery combined with oxaliplatin-based chemotherapies (oxaliplatin + 5-fluoro-uracyl, 5-FU), and only in a few cases anti-HER2 or anti-PD1 targeted therapies are applied.[51,52] Consequently, there is urgent need for the development of new therapeutic solution to improve the management of gastric cancer patients. In this respect, components of the Hippo pathway, like MST2, or the S6K1 signaling pathway have been reported to be frequently altered in GC and are subjects to the development of targeted therapies.[53–55] To investigate the inhibitory effect of our compounds on the protein kinase MST2, we chose to analyze the phosphorylation state of YAP, a downstream in the Hippo pathway. For this AGS cell were treated for 24 h with the indicated compounds at 2 or 25 μM concentrations, and the expression of YAP and phosphorylated YAP was analyzed by western blot (Fig. 12a).

The results show that among the four compounds tested only **Ru(3)** at 25 μM significantly diminished the phosphorylation of YAP, suggesting inhibition of the upstream protein kinase MST2. By contrast, **Ru(5)** and **Pt(3)** showed only a very slight effect, which did not reach statistical significance, and **Pt(4)** showed the opposite effect (Fig. 12). This result is in contradiction with the positive docking score obtained from the modeling of **Ru(3)** in the binding pocket of MST2. However, since the acetonitrile ligands responsible for steric clashing with the protein are effectively exchanged with less bulky substituents such as water in a biologically relevant medium (see above), it is possible that the product of such ligand exchange is a good fit in the protein binding pocket. This was confirmed by new docking experiments where the acetonitrile ligands were exchanged from water or DMSO ligands. These modeled

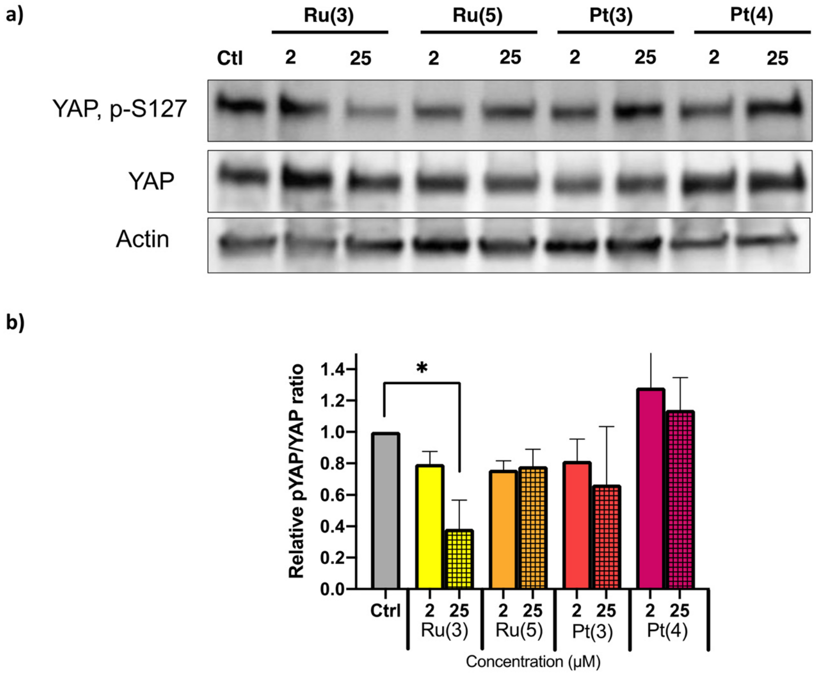

Fig. 12 (a) AGS cells were treated for 24 h with 2 or 25 μM of the indicated drugs and the expression of YAP and YAP p-S127 was analyzed by western blot. The expression of actin served as a loading control. Western blot analysis of YAP. The same blot was first probed with an antibody detecting phosphorylated YAP (mouse monoclonal antibody) and then re-probed with an antibody detecting total YAP (rabbit-monoclonal antibody), ensuring accurate comparison while eliminating variability due to loading and migration differences. (b) Relative pYAP and YAP expression levels were normalized to the corresponding actin expression levels and are represented as ratio pYAP/YAP. The results are given ± SEM from three distinct experiments. Statistical difference was established by a two-value's *t* test. *$p < 0.05$.

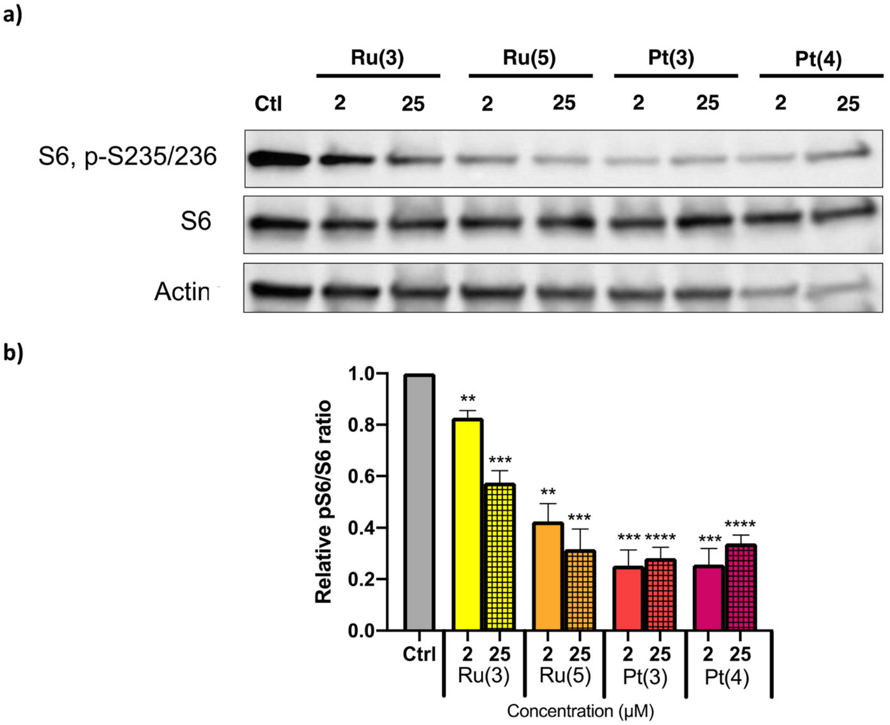

Fig. 13 (a) AGS cells were treated for 24 h with 2 or 25 μM of the indicated drugs and the expression of S6 and p-S6 was analyzed by western blot. The expression of actine served as a loading control. The nitrocellulose blot was successively probed and revealed for S6 p-S235/236, S6 and actin (b) relative pS6 and S6 expression levels where normalized with the corresponding actin expression level and are represented as ratio pS6/S6. The results are given ± SEM from three distinct experiments. Statistical difference was established by a two-value's *t* test. *$p < 0.05$, **$p < 0.01$, ***$p < 0.005$, ****$p < 0.001$.

complexes are named **Ru(3)–H_2O** and **Ru(3)–DMSO** and the docking scores obtained for these two complexes with the binding pocket of MST2 are found in Table 3. The negative docking score for **Ru(3)–H_2O** (−57.8) demonstrates that this aqua adduct well fits the binding pocket of the enzyme and has significant affinity. By contrast, the DMSO adduct (**Ru-DMSO**) has an unfavorable docking score (+12.7) similar as the **Ru(3)** species. Clearly, this investigation demonstrates that the efficacy of **Ru(3)** is enhanced by water and not DMSO substitution. Additionally, the binding mode of Ru–H_2O predicted by docking resembles that of staurosporine with two H-bonding interactions with the same protein loop.

Next, we evaluated the inhibitory activity of the four complexes on S6K1 by analyzing the protein expression of S6 and its phosphorylated analogue p-S6. For this purpose, AGS cells were treated for 24 h with 2 or 25 μM of **Ru(3)**, **Ru(5)**, **Pt(3)** and **Pt(4)** and the expression of S6 and p-S6 analyzed by western blot (Fig. 13a).

The results show that, in contrast to the YAP phosphorylation, all compounds significantly decrease the phosphorylation of S6, suggesting S6K1 inhibition at 25 μM concentration (Fig. 13). Interestingly and in contrast to the previous results on YAP phosphorylation, **Pt(3)** showed to be much more potent than **Ru(3)** to inhibit S6K1. Overall, the Pt(ii) complexes seemed to be more efficient in inhibiting the activity of the protein kinase S6K1 than the Ru(ii) complexes. These observations are consistent with conclusions drawn from the docking experiments, as the Pt(ii) complexes have lower docking scores than the Ru(ii) complexes in the S6K1 binding pocket (Table 3). Since the S6K1 binding pocket is bigger than the MST2 binding pocket, these data confirm that bulkier complexes such as the Pt(ii) complexes, in comparison to the Ru(ii) complexes, will have stronger interactions with larger protein binding pockets.

Conclusion

Five Ru(ii) complexes, *i.e.* **Ru(1)–(5)**, and four Pt(ii) complexes, *i.e.* **Pt(1)–(4)**, were generated from ligands $\mathbf{L_1}$ and $\mathbf{L_2}$ that incorporate a NH–CO fragment. All of these species are stable in aqueous media with the exception of **Ru(3)** where the labile acetonitrile ligands are substituted. Complexes **Ru(1)**, **Ru(2)**, **Ru(4)**, **Pt(1)** and **Pt(2)** are toxic molecules for AGS cells, whereas compounds **Ru(3)**, **Ru(5)**, **Pt(3)** and **Pt(4)** displayed IC_{50} > 200 μM. Hence, the non-toxic species (**Ru(3)**, **Ru(5)**, **Pt(3)** and **Pt(4)**) were selected for docking studies in two protein kinases, *i.e.* MST2 and S6K1. From this investigation, it appeared that all complexes could fit the ATP-binding pocket of these enzymes. Nevertheless, docking results predicted that platinum compounds have stronger affinities for the ATP-binding pocket of S6K1. Finally, inhibitory activities *in vitro* using the gastric cancer cell line AGS were evaluated. It was found that **Ru(3)** at 25 μM significantly diminished the phosphorylation of YAP, suggesting that it inhibited the activity of the upstream protein kinase MST2. Albeit in contradiction with the docking results, which indicated that this compound would not fit the ATP-binding pocket of MST2, this observation along with the detected lability of the acetonitrile ligands within **Ru(3)** in water suggest that the active form of this compound may be water or DMSO coordinated. Concerning the inhibition of S6K1, the two platinum species showed the best activities, consistent with the docking predictions.

Overall, albeit the structure of the ATP binding pockets of protein kinases are similar, this investigation has highlighted a preferred interaction for a particular type of kinase depending on the architecture and the substitution of the metal complex inhibitor. These results open to the development of selective metal complex kinase inhibitors based on the diimine ligand L_2.

Experimental part

Materials and methods

Antibodies list: ESI.‡

Synthetic procedures

All reagents and products were purchased from Sigma Aldrich, Alfa Aesar or TCI and used as received. Ultrapure water used was purified by a Milli-Q UV purification system (Sartorius Stedim Biotech SA). Gibco® Versene solution, Gibco® Trypsin/EDTA solution, Gibco® MEM Non-Essential Amino Acids solution (NEAA), 10% SDS solution, PenicillinStreptomycin (10 000 U mL^{-1}), Dulbecco's Phosphate-Buffered Saline (10×). Hyclone™ RPMI 1640, DMEM medium and fetal bovine serum (FBS) were purchased from Thermo Fisher Scientific Inc. Bio-rad Protein Assay Dye Reagent Concentrate, 40% acrylamide/bis solution, 10× Tris/glycine buffer, TEMED, 4× Laemmli Sample Buffer, nitrocellulose membrane, 0.2 μm and 0.45 μm were purchased from Bio-rad Laboratories. Complete™, mini Protease Inhibitor Cocktail Tablets. Luminata™ Classico and Luminata™ Crescendo Western HRP Substrate were purchased from Merck Millipore Corporation.

Bruker Avance-500 and Avance-600 spectrometers were used for solution NMR analyses performed at 25 °C. Deuterated solvents for ^{1}H NMR analysis were dried over molecular sieves before use. ^{1}H NMR spectra were recorded at 500.13 MHz and referenced to $SiMe_4$. $^{13}C\{^1H\}$ NMR spectra (broadband decoupled) were recorded at 125.77 MHz and referenced to $SiMe_4$. Chemical shifts are reported in ppm and coupling constants in Hz; the latter are proton–proton coupling constants. Multiplicity: s = singlet, d = doublet, t = apparent triplet, m = multiplet. The $^{13}C\{^1H\}$ signals are singlets. DOSY measurements were performed at 600.13 MHz with a 5 mm ^{1}H/X *z*-gradient BBI probe and applying a PFGSTE pulse sequence using bipolar gradients. Electrospray analyses were performed on a MicroTOF (Bruker) apparatus equipped with an electrospray (ES) source. The elemental analyses were performed using a Flash 2000 apparatus (Thermo Fisher Scientific) for C, H, and N elements. UV-vis liquid and solid spectra were recorded with a PerkinElmer Lambda650s spectrometer. The X-ray diffraction data were collected by two different means. *Mean 1*: the data were collected at and 173 K on a Bruker SMART CCD diffractometer with MoKα radiation (λ = 0.71073 Å). The diffraction data were corrected for absorption using the SADABS program.[56] The structures were solved using SHELXS97[57] and refined by full matrix least-squares on F^2 using SHELXL-2014[58] in the anisotropic approximation for all non-hydrogen atoms. The hydrogen atoms were introduced at calculated positions and not refined (riding model). *z* with a 5 mm 1H/X *z*-gradient BBI probe and applying a PFGSTE pulse sequence using bipolar gradients. *Mean 2*: the X-ray diffraction data were collected on a Bruker PHOTON-III DUO Kappa CPAD diffractometer equipped with an Oxford Cryosystem liquid N_2 device, using Mo-Kα radiation (λ = 0.71073 Å). The crystal-detector distance was 37 mm. The cell parameters were determined (APEX3 software)[59] from reflections taken from two sets of 6 frames, each at 10 s exposure. The structure was solved by Direct methods using the program SHELXT-2014. The refinement and all further calculations were carried out using SHELXL-2014. The H-atoms were included in calculated positions and treated as riding atoms using SHELXL default parameters. The non-H atoms were refined anisotropically, using weighted full-matrix least-squares on F^2. A semi-empirical absorption correction was applied using SADABS in APEX3. The residual electron density was assigned to one molecule of the chloroform solvent. Absorbance and fluorescence on 96-well plates were measured using Tristar^2 Multimode Reader LB942 from Berthold Technologies.

Cell culture and cell survival

AGS (CRL-1739™), and KATOIII (HTB-103TM) cells were obtained from ATCC. 0.5 × 10^4 cells were seeded per well in 96-well microplates (Falcon Multiwell), 24 h prior to any treatment, drugs were added in fresh medium for 48 h. Then the medium was replaced by fresh medium supplemented with 0.5 mg mL^{-1} MTT (Sigma) for 1 h. Subsequently, the medium was aspirated, and the purple formazan crystals were dissolved in DMSO (100 μL). Absorbance was measurements at 590 nm with the LB942 Tristar2 Multimode Reader (Berthold Technologies). The IC_{50} and IC_{75} was calculated with Prism 9.5.0 using non-linear regression. The experiments were performed in 4 replicates for each drug concentration and were carried out at least three times independently.

Western blot protocol

AGS cells were grown at 500 000 cells per well (2 mL) on Cellstar® 6-well plates (Greiner Bio-One) for **24 h or 17 h** cells were lysed with NP40 Lysis Buffer (125 mM TrisHCl pH 7.5, NaCl 150 mM, NP40 0.5%, 10% Glycerol). A total of 50 μg of proteins were resolved by 10% or 15% SDS-PAGE (depending on protein molecular weight) according to standard methods.

Proteins were visualized with selected antibodies (see ESI Methods‡) and enhanced chemiluminescence using the Luminata™ Classico and Luminata™ Crescendo western blotting Substrate Millipore reagent, and according to the manufacturer instructions. To evaluate the phosphorylation of YAP at S127 and S6 at S235/236, the same blot was first probed with an antibody detecting the phosphorylated protein and then re-probed with an antibody detecting the total protein, ensuring accurate comparison while eliminating variability due to loading and migration differences. For instance, for YAP, the blot was probed first with the mouse monoclonal antibody directed against the phosphorylated protein (YAP, anti-rabbit, S127-D9W2I Cell Signaling; in 1/1000 in TBS 1×, Tween 20 0.1%, BSA 1%) overnight, then it was washed (TBS 1×, Tween 20 0.1%, BSA 1%) 3 times 5 min and probed with the anti-mouse secondary antibody (sc-101190 Santa Cruz, 1/5000 in TBS 1×, Tween 20 0.1%, BSA 1%) before revelation with ECL. The same blot was thoroughly washed (TBS 1×, Tween 20 0.1%, BSA 1%) and then probed for the whole protein with an antibody that have been produced in rabbit to avoid any cross-reaction with the mouse phospho-antibody previously used. The use of two antibodies produced in different species avoid the cross-reaction and the necessity of stripping that may lead to a protein loss on the blot. The ECL signals were acquired on a Pxi Imager (Syngene®). Expression intensities of the protein of interest were measured using ImageJ software and normalized to their respective loading control (Actine). Finally, the protein of interest to loading control ratios were further normalized by setting the value of this ratio to 1 in the negative control.

Molecular docking

The initial coordinates of the MST2 protein were taken from the crystal structure of MST2 solved in complex with the inhibitor 4-[(5,10-dimethyl-6-oxo-6,10-dihydro-5*H*-pyrimido[5,4-*b*]thieno[3,2-*e*][1,4]diazepin-2-yl)amino]benzenesulfonamide, a.k.a. XMU-MP-1 or 5BS (PDB code: 5DH3). The initial coordinates of the S6K1 protein were taken from the crystal structure of S6K1 solved in complex with the ruthenium complex FL772 (PDB code: 4RLP). Starting from 2D chemical structures, PrepFlow provides 3D molecular coordinates, after tautomer, stereoisomer and conformer enumeration at a given pH, here 7.0. All docking experiments were performed using the program PLANTS in combination with the scoring function CHEMPLP, which includes energy contributions accounting for hydrogen bonding, protein–ligand shape complementarity, and intra-ligand torsion and clash penalties. The searching space for docking was defined based on the center of mass of the co-crystallized ligand and a sphere radius of 8.0 Å. For each compound, 10 binding poses were generated. The best binding mode according to the docking score was selected and analyzed as the most representative binding pose.

Ru(1)

In a two-necked round-bottom flask, a mixture of ethylene glycol and water (9 : 1, 3 mL) was degassed for 15 min by Ar bubbling. **1** (50 mg, 103 μmol) and **L_1** (28 mg, 103 μmol) were added and the mixture was stirred at 120 °C for 6 h with light excluded. The orange mixture was cooled to r.t. and water (4.5 mL) was added. An aqueous saturated solution of KPF_6 was added drop by drop until no precipitate formed anymore. The orange solid was filtered, washed with cold water and diethyl ether. The crude product was purified by column chromatography (SiO_2, MeCN : water : KNO_3, 100 : 10 : 1). The fractions containing product were combined and the solvent was removed *in vacuo*. The residue was dissolved in MeCN, the excess KNO_3 was filtered off and an aqueous saturated solution of KPF_6 was added. The solution was concentrated until a precipitate formed. The precipitate was filtered, washed with cold water and diethyl ether to isolate **Ru(1)** (56 mg, 56%). ^{1}H NMR (CD_3CN, 500 MHz): δ (ppm) = 8.58–8.49 (m, 7H), 8.15 (s, 1H), 8.12–8.08 (m, 4H), 8.02–7.98 (m, 2H), 7.86–7.84 (m, 2H), 7.75–7.65 (m, 3H), 7.59–7.58 (m, 2H), 7.55–7.53 (m, 1H), 7.47–7.44 (m, 2H), 6.61 (d, 1H). ^{13}C NMR (126 MHz, CD_2Cl_2): δ = 162.45, 157.80, 157.76, 157.57, 157.56, 152.95, 152.92, 152.56, 152.53, 152.48, 152.38, 148.68, 147.62, 143.04, 138.41, 138.40, 138.31, 138.29, 137.08, 136.81, 136.26, 135.64, 131.00, 130.93, 128.10, 128.05, 127.97, 127.93, 126.92, 126.42, 124.83, 124.80, 124.75, 121.20 ppm. MS (ESI) calcd for $C_{37}H_{27}N_7ORu^{2+}$ 343.57; found 343.57. Anal. calcd for $C_{37}H_{27}F_{12}N_7OP_2Ru\cdot H_2O$: C, 44.68; H, 2.94, N, 9.86; found C, 44.17; H, 2.93; N, 9.65.

Ru(2)

In a two-necked round-bottom flask, a mixture of ethylene glycol and water (9 : 1, 3 mL) was degassed for 15 min by Ar bubbling. **1** (50 mg, 103 μmol) and **L_2** (20 mg, 103 μmol) were added and the mixture was stirred at 120 °C for 6 h with light excluded. The orange mixture was cooled to r.t. and water (4.5 mL) was added. An aqueous saturated solution of KPF_6 was added drop by drop until no precipitate formed anymore. The orange solid was filtered, washed with cold water and diethyl ether. The crude product was purified by column chromatography (SiO_2, MeCN : water : KNO_3 100 : 10 : 1). The fractions containing product were combined and the solvent was removed *in vacuo*. The residue was dissolved in MeCN, the excess KNO_3 was filtered off and an aqueous saturated solution of KPF_6 was added. The solution was concentrated until a precipitate formed. The precipitate was filtered, washed with cold water and diethyl ether to isolate **Ru(2)** (51 mg, 81%). Crystals were obtained from acetone/Et_2O. T = 296(2) K; monoclinic; space group $P2_{1/c}$; a = 13.4931(5) Å, b = 13.8886(4) Å, c = 19.9737(8) Å; β = 94.6980(10); V = 3730.5(3) Å^3; Z = 4; D_{calcd} = 1.707 g cm^{-3}; reflections collected: 35 303; R_{int} = 0.0671; $R_1(F)$ ($I > 2\sigma(I)$) = 0.0637, w$R_2(F^2)$ (all data) = 0.1935; GOF(F^2) = 1049. CCDC: 2392833. ^{1}H NMR (CD_3CN, 500 MHz): δ (ppm) = 8.68 (dd, 1H, ^3J = 8.1 Hz, ^4J = 1.2 Hz, $\mathbf{H_4}$), 8.52–8.48 (m, 4H, $\mathbf{H_2}$ + $\mathbf{H_{bpy}}$), 8.10–8.03 (m, 5H), 7.95 (dd, 1H, ^3J = 8.3 Hz, ^4J = 1.2 Hz), 7.80–7.77 (m, 2H), 7.74–7.71 (m, 2H), 7.55–7.50 (m, 2H), 7.44–7.41 (m, 2H), 7.37–7.33 (m, 2H). ^{13}C NMR (126 MHz, CD_3CN): δ (ppm) = 160.58, 158.20, 157.87, 157.85, 156.98, 155.16, 153.31, 153.26, 153.08, 152.96, 147.63, 139.27, 138.93, 138.90, 137.58, 136.99, 129.55, 128.55, 128.50, 128.49, 128.47, 128.24, 127.36, 125.25, 125.19, 125.15, 124.84. MS (ESI) calcd for $C_{31}H_{23}N_7ORu^{2+}$ 305.55; found 305.55. Anal. calcd for $C_{31}H_{23}F_{12}N_7OP_2Ti$: C, 41.34 H, 2.57, N, 10.89; found C, 40.28; H, 2.72; N, 10.25.

Ru(3)

In a two-necked round-bottom flask, MeCN (5 mL) was degassed by argon bubbling for 15 min. **2** (50 mg, 100 μmol) and $\mathbf{L_2}$ (20 mg, 100 μmol) were added and the mixture was stirred at 30 °C for 48 h, then 40 °C for 24 h and finally 45 °C for 48 h. The mixture was filtered, and the purple solution was purified by column chromatography (SiO_2, MeCN : water : KNO_3 100 : 3 : 1). The red band was recovered, the fractions were combined, and the solvent was removed *in vacuo*. The residue was redissolved in a minimum of MeCN, and an aqueous saturated KPF_6 was added (2 mL). MeCN was removed to obtain a dark precipitate which was filtered and washed with ether to isolate **Ru(3)** (12 mg, 18%). ^{1}H NMR ($CDCl_3$, 500 MHz): δ (ppm) = 11.33–11.24 ($\mathrm{m_{br}}$, 2H, **N–H**), 9.79 (d, 1H, ^3J = 5 Hz, $\mathbf{H_2}$), 9.27 (d, 1H, ^3J = 4.7 Hz, $\mathbf{H_{2'}}$), 8.87 (d, 1H, ^3J = 5.4 Hz, $\mathbf{H_{9'}}$), 8.83 (d, 1H, ^3J = 8 Hz, $\mathbf{H_4}$), 8.62 (d, 1H, ^3J = 7.9 Hz, $\mathbf{H_{7'}}$), 8.40 (d, 1H, ^3J = 5.3 Hz, $\mathbf{H_9}$), 8.13 (dd, 1H, $^3J_1$ = 7.8 Hz, $^3J_2$ = 5.3 Hz $\mathbf{H_3}$), 8.05 (d, 1H, $^3J_1$ = 8.2 Hz, $\mathbf{H_{4'}}$), 7.96 (dd, 1H, $^3J_1$ = 8.1 Hz, $^3J_2$ = 4.9 Hz $\mathbf{H_{3'}}$), 7.86–7.81 (m, 3H, $\mathbf{H_{7,a,a'}}$), 7.46 (dd, 1H, $^3J_1$ = 7.7 Hz, $^3J_2$ = 5.7 Hz $\mathbf{H_{8'}}$), 7.35 (dd, 1H, $^3J_1$ = 8.2 Hz, $^3J_2$ = 5.4 Hz $\mathbf{H_8}$), 7.26–7.21 (m, 2H, $\mathbf{H_{b,b'}}$), 7.09–7.07 (m, 2H, $\mathbf{H_{d,d'}}$), 6.99–6.94 (m, 2H, $\mathbf{H_{c,c'}}$), 3.94 (m, 2H, $\mathbf{H_{f,f'}}$), 3.34 (d, 1H, ^3J = 5 Hz, $\mathbf{H_g}$), 3.31 (d, 1H, ^3J = 5 Hz, $\mathbf{H_{g'}}$), 2.55 (m, 6H, **MeCN**), 2.31 (s, 6H, $\mathbf{H_{h,h'}}$), 2.11 (s, 3H, **MeCN**), 2.10 (s, 3H, **MeCN**), 1.42 (s, 3H, $\mathbf{H_i}$), 1.40 (s, 3H, $\mathbf{H_{i'}}$). ^{13}C NMR ($CDCl_3$, 126 MHz): δ (ppm) = 161.83, 161.28, 157.51, 156.64, 156.11, 152.38, 148.95, 147.68, 146.91, 141.01, 137.41, 136.85, 135.13, 135.12, 134.62, 133.71, 128.87, 128.08, 127.54, 126.63, 125.21, 125.10, 124.63, 123.54, 122.56, 120.73, 120.60, 73.30, 52.85, 52.78, 51.41, 51.09, 4.83, 4.21, 4.20. MS (ESI) calcd for $C_{24}H_{25}N_6ORu^+$ 515.11, found 515.11. Anal. calcd for $C_{24}H_{25}F_6N_6OPRu\cdot 2\ CH_2Cl_2$: C, 37.65; H, 3.52; N, 10.13; found C, 35.94; H, 3.50; N, 10.17.

Ru(4)

In a two-necked round-bottom flask, MeOH (10 mL) was degassed by argon bubbling for 15 min. **3** (95 mg, 149 μmol) and $\mathbf{L_2}$ (29 mg, 149 μmol) were added and the mixture was stirred at 70 °C overnight. The mixture was cooled down at room temperature and the solvent was removed *in vacuo*. The residue was purified by column chromatography (Al_2O_3, MeCN : water 99 : 1). The red band was recovered, the fractions were combined, and the solvent was removed *in vaccuo* to isolate a purple crystalline powder (20 mg, 18%). ^{1}H NMR ($CDCl_3$, 500 MHz): δ (ppm) = 10.07 ($\mathrm{s_{br}}$, 2H, **N–H + N–H′**), 8.64 (dd, 1H, ^3J = 8.1 Hz, ^4J = 1.3 Hz, H_{57}), 8.46 (dd, ^3J = 8 Hz, ^4J = 1.4 Hz, $H_{57'}$), 8.32–8.30 (m, 5H), 8.26 (dd, 1H, ^3J = 5.6 Hz, ^4J = 1.4 Hz, $H_{57'}$), 8.22 (dd, ^3J = 5.3 Hz, ^4J = 1.4 Hz, H_{57}), 8.02–7.99 (m, 2H), 7.87–7.78 (m, 13H), 7.75 (dd, 1H, ^3J = 5.2 Hz, ^4J = 1.1 Hz), 7.70–7.66 (m, 6H), 7.62 (dd, 1H, ^3J = 8.4 Hz, ^4J = 1 Hz), 7.58–7.55 (m, 4H), 7.48 (dd, 1H, $^3J_1$ = 5.6 Hz, $^3J_2$ = 8.1 Hz, $\mathbf{H_{phen'}}$), 7.36 (dd, 1H, $^3J_1$ = 5.5 Hz, $^3J_2$ = 8.4 Hz), 7.18–7.14 (m, 2H), 6.92–6.83 (m, 7H), 6.47–6.43 (m, 2H). ^{13}C NMR (CD_3CN, 126 MHz): δ (ppm) = 167.67, 160.71, 160.63, 158.50, 157.42, 157.38, 157.33, 155.58, 153.98, 152.97, 151.53, 151.48, 151.15, 151.04, 150.95, 149.50, 144.57, 137.52, 136.80, 136.60, 136.43, 136.39, 136.09, 135.09, 134.68, 134.55, 133.56, 128.99, 128.75, 128.02, 127.49, 126.89, 126.87, 126.86, 126.67, 126.64, 126.61, 126.28, 124.65, 123.57, 123.53, 123.48, 122.89, 122.83, 122.82, 121.45, 119.37, 119.32. MS (ESI) calcd for $C_{32}H_{23}N_6ORu^+$ 609.10, found 609.10. Anal. Calcd for $C_{32}H_{23}F_6N_6OPRu\cdot 2\ CH_2Cl_2$: C, 44.22; H, 2.95, N, 9.10; found C, 43.50; H, 2.93; N, 9.31.

Ru(5)

A solution of **4** (61 mg, 122 μmol) and $\mathbf{L_2}$ (50 mg, 254 μmol) was heated to reflux in MeOH (21 mL) for 4 h. Solvent was removed *in vacuo* and the residue was redissolved in water (10 mL). The unsoluble material was filtered off and a saturated aqueous solution of KPF_6 was added until no precipate formed anymore. The precipitate was filtered on a fritted funnel, washed with water (3 × 10 mL), with Et_2O (3 × 10 mL) to obtain a yellow powder. ^{1}H NMR (CD_3CN, 500 MHz): δ (ppm) = 9.95 (dd, 1H, ^3J = 5.4 Hz, ^4J = 1.3 Hz, $\mathbf{H_2}$), 9.18 (dd, 1H, ^3J = 5.3 Hz, ^4J = 0.9 Hz, $\mathbf{H_9}$), 8.81 (dd, 1H, ^3J = 8.1 Hz, ^4J = 1.31 Hz, $\mathbf{H_4}$), 7.97–7.93 (m, 2H, $\mathbf{H_{3,7}}$), 7.80 (dd, 1H, ^3J = 8.1 Hz, ^4J = 1.31 Hz, $\mathbf{H_8}$), 6.07 (s, 6H, $\mathbf{H_{benz}}$). ^{13}C NMR (CD_3CN, 126 MHz): δ (ppm) = 159.59, 159.38, 152.83, 150.39, 139.04, 137.12, 136.53, 129.10, 127.87, 126.48, 126.42, 87.16. MS (ESI) calcd for $C_{17}H_{13}ClN_3ORu^+$ 411.98, found 411.98. Anal. calcd for $C_{17}H_{13}ClF_6N_3OPRu$: C, 36.67; H, 2.35; N, 7.55; found C, 36.51; H, 2.48; N, 7.53.

Pt(1)

5 (48 mg, 126 μmol) and $\mathbf{L_1}$ (35 mg, 126 μmol) were suspended in distilled water (12 mL) and the mixture was stirred at reflux for three days. The clear yellow solution was concentrated *in vacuo* until the volume reached around 2 mL. The product was purified on a Porapak Rxn RP 20cc column with water as eluent. The fractions containing product were combined, concentrated *in vacuo* until the volume reached around 3 mL. Saturated aqueous KPF_6 was added to the solution until no precipate formed anymore. The yellow residue was filtered on a fritted funnel, and air-dried. Yield: 20%. ^{1}H NMR (CD_3CN, 500 MHz): δ (ppm) = 8.94–8.89 (m, 4H, $\mathbf{H_{2,4,7,9}}$), 8.15 (s, 1H, $\mathbf{H_6}$), 8.08 (dd, 1H, $^3J_1$ = 8.3 Hz, $^3J_2$ = 5.4 Hz, $\mathbf{H_{3\ or\ 8}}$), 8.06 (dd, 1H, $^3J_1$ = 8.6 Hz, $^3J_2$ = 5.4 Hz, $\mathbf{H_{3\ or\ 8}}$), 7.63 (dd, 1H, ^3J = 9.4 Hz, ^4J = 2.7 Hz, $\mathbf{H_{pyr}}$), 7.58 (d, 1H, ^4J = 2.6 Hz, $\mathbf{H_{pyr}}$), 6.63 (d, 1H, ^3J = 9.5 Hz, $\mathbf{H_{pyr}}$), 5.82 ($\mathrm{s_{br}}$, 2H, $\mathbf{NH_2}$), 5.17 ($\mathrm{s_{br}}$, 2H, $\mathbf{NH_2}$), 2.78 (m, 2H, $\mathbf{H_{DACH}}$), 2.25 (m, 2H, $\mathbf{H_{DACH}}$) 1.71 (m, 2H, $\mathbf{H_{DACH}}$), 1.53 (m, 2H, $\mathbf{H_{DACH}}$), 1.31 (m, 2H, $\mathbf{H_{DACH}}$). ^{13}C NMR (CD_3CN, 126 MHz): δ (ppm) = 162.89, 152.63, 152.47, 149.04, 147.85, 143.28, 142.09, 140.64, 137.57, 137.15, 131.68, 128.39, 127.78, 127.39, 121.81, 114.91, 62.88, 62.84, 33.15, 24.87. HRMS (ESI) calcd for $C_{23}H_{24}N_5OPt^{2+}$ 291.0849, found 291.0862.

Pt(2)

5 (77 mg, 203 µmol) and **L$_2$** (40 mg, 203 µmol) were suspended in distilled water (18 mL) and the mixture was stirred at reflux overnight. The clear yellow solution was concentrated *in vacuo* until the volume reached around 2 mL. The product was purified on a Porapak Rxn RP 20cc column with water as eluent. The fractions containing product were combined and dried *in vacuo* to obtain a yellow solid. Yield: 39%. ^{1}H NMR (D_2O, 500 MHz): δ (ppm) = 9.01 (d, 1H, ^3J = 8.1 Hz, H$_4$), 8.95 (d, 1H, ^3J = 5.6 Hz, H$_2$), 8.50 (d, 1H, ^3J = 5.3 Hz, H$_9$), 8.20 (d, 1H, ^3J = 8.6 Hz, H$_7$), 8.01 (dd,1H, $^3J_1$ = 5.7 Hz, $^3J_2$ = 8.06 Hz, H$_3$), 7.87 (dd, 1H, $^3J_1$ = 5.4 Hz, $^3J_2$ = 8.5 Hz, **H$_8$**), 2.71–2.69 (m, 2H, **H$_{DACH}$**), 2.21 (d, 2H, ^3J = 13 Hz, **H$_{DACH}$**), 1.66 (d, 2H, ^3J = 8.8 Hz, **H$_{DACH}$**), 1.47 (d, 2H, ^3J = 9.2 Hz, **H$_{DACH}$**), 1.29–1.20 (q, 2H, ^3J = 13 Hz, **H$_{DACH}$**) ppm. ^{13}C NMR (D_2O, 125 MHz): δ (ppm) = 161.08, 154.52, 154.50, 145.86, 139.87, 138.88, 135.44, 129.08, 128.56, 127.77, 125.51, 61.67, 61.64, 32.01, 31.97, 23.75 ppm. MS (ESI) calcd for $C_{17}H_{21}N_5OPt^{2+}$ 253.07; found 253.07. Anal. calcd for $C_{17}H_{21}Cl_2N_5OPt \cdot 2\ H_2O$: C, 33.29; H, 4.11; N, 11.42; found C, 32.22; H, 4.10; N, 11.05.

Pt(3)

6 (60 mg, 158 µmol) was dissolved in DMF (4 mL). $AgNO_3$ (59 mg, 347 µmol) was added and the mixture was stirred for 16 h with light excluded. The mixture was centrifuged for 5 min at 4000 rpm. To the supernatant was added **L$_2$** (37 mg, 189 µmol) and the mixture was stirred for 16 h and then for 24 h at 50 °C. The yellow mixture was cooled to room temperature and centrifuged for 5 min at 4000 rpm. The yellow precipitate was washed with CH_2Cl_2 (3 × 5 mL) and air-dried. The residue was dissolved in water (10 mL), filtered and a saturated aqueous solution of KPF_6 was added. The solution was concentrated *in vacuo* until a precipate appeared. The mixture was allowed to rest O.N. with light excluded. The solid was centrifuged 5 min at 4000 rpm, the solid was washed with a 50 : 50 mixture of iPrOH : Et_2O and air-dried. Yield: 16%. ^{1}H NMR (DMSO-d_6, 500 MHz): δ (ppm) = 8.83 (d, 1H, ^3J = 8.01 Hz, **H$_4$**), 8.64 (d, 1H, ^3J = 5.2 Hz, **H$_2$**), 7.99 (dd, $^3J_1$ = 7.8 Hz, $^3J_2$ = 5.8 Hz, **H$_3$**), 7.93–7.88 (m, 2H, **H$_{7/9}$**), 7.69 (dd, $^3J_1$ = 8.6 Hz, $^3J_2$ = 5.2 Hz, **H$_8$**), 6.52 (s, 4H, **NH$_2$**), 3.44 (s$_{br}$, 2H, **CH**–NH$_2$), 1.8–1.72 (m, 8H). ^{13}C NMR (DMSO-d_6, 126 MHz): δ (ppm) = 167.11, 154.11, 149.51, 140.46, 138.55, 137.86, 135.41, 126.65, 126.28, 125.11, 46.93, 46.83, 21.75, 21.70. MS (ESI) calcd for $C_{17}H_{20}N_5OPt^+$ $[M - H]^+$ 505.13, found 505.13.

Pt(4)

8 (50 mg, 108 µmol) and (1*S*,2*S*)-**9** (46 mg, 216 µmol) were suspended in water (100 mL) and stirred for 24 h at reflux. The mixture was allowed to cool at room temperature and was concentrated *in vacuo* until 50 mL solvent remained. A saturated aqueous solution of KPF_6 was added until no precipate formed anymore. The mixture was filtered on a fritted funnel, washed with water and Et_2O to obtain a yellow powder. Yield: 38%. Crystals were obtained from MeCN/Et_2O. T = 296(2) K; orthorhombic; space group P212121; a = 6.6613(4) Å, b = 16.7503(10) Å, c = 32.2265(18) Å; $\alpha = \beta = \gamma = 90°$; V = 3595.8(4) Å^3; Z = 4; D_{calcd} = 1.518 g cm^{-3}; reflections collected: 106 407; R_{int} = 0.0807; $R_1(F)$ ($I > 2\sigma(I)$) = 0.0556, w$R_2(F^2)$ (all data) = 0.1337; GOF(F^2) = 1.118. CCDC: 2392834.‡ ^{1}H NMR (CD_3CN, 500 MHz): δ (ppm) = 8.75 (d, 1H, ^3J = 8 Hz, **H$_4$**), 8.13 (d, 1H, ^3J = 5.2 Hz, **H$_2$**), 7.73 (d, 1H, ^3J = 8.6 Hz, **H$_7$**), 7.67–7.66 (m, 5H, **H$_9$, H$_{Ph}$**), 7.39–7.33 (m, 7H, **H$_3$, H$_{Ph}$**), 7.13 (dd, 1H, $^3J_1$ = 8.4 Hz, $^3J_2$ = 5.2 Hz, **H$_8$**), 6.43–6.09 (m$_{br}$, 4H, **NH$_2$**), 4.86 (s, 2H, **CH**–NH$_2$). ^{13}C NMR (CD_3CN, 126 MHz): δ (ppm) = 168.89, 152.96, 152.09, 147.05, 142.17, 140.29, 137.70, 136.24, 136.16, 135.23, 130.11, 130.09, 129.74, 129.72, 129.02, 128.95, 127.56, 127.24, 126.30, 66.76, 66.47. $[\alpha]_D$ = 5.8° dm^{-1} cm^3 g^{-1} (c = 0.67 mM, DMSO, 20 °C). MS (ESI) calcd for $C_{25}H_{23}N_5OPt^{2+}$ 302.08, found 302.08. Anal. calcd for $C_{25}H_{23}F_{12}N_5OP_2Pt \cdot 2MeCN \cdot C_5H_{12}$: C, 38.31; H, 3.80; N, 9.48; found C, 39.13; H, 3.41; N, 9.12.

Data availability

The data supporting this article have been included as part of the ESI.‡

Crystallographic data for **Ru(2)** and **Pt(4)** has been deposited at the CCDC 2392833 and 2392834‡ respectively.

Conflicts of interest

There are no conflicts to declare.

Acknowledgements

We thank the University of Strasbourg and the CNRS for financial support. This research has been supported by the University of Strasbourg's IdEx program (Idex-CNRS interdisciplinary project 2017). M. Scarpi-Luttenauer thanks the French Ministry of Research for his PhD fellowship. CG, GM and CO are supported by ARC, Ligue contre le Cancer, ITMO cancer, INCa and the ITI Innovec.

References

1 G. Manning, D. B. Whyte, R. Martinez, T. Hunter and S. Sudarsanam, The Protein Kinase Complement of the Human Genome, *Science*, 2002, **298**(5600), 1912–1934, DOI: **10.1126/science.1075762**.

2 H. J. Su Huang, M. Nagane, C. K. Klingbeil, H. Lin, R. Nishikawa, X. D. Ji, C. M. Huang, G. N. Gill, H. S. Wiley and W. K. Cavenee, The Enhanced Tumorigenic Activity of a Mutant Epidermal Growth Factor Receptor Common in Human Cancers Is Mediated by Threshold Levels of Constitutive Tyrosine Phosphorylation and Unattenuated Signaling, *J. Biol. Chem.*, 1997, **272**(5), 2927–2935, DOI: **10.1074/jbc.272.5.2927**.

3 A. J. Wong, S. H. Bigner, D. D. Bigner, K. W. Kinzler, S. R. Hamilton and B. Vogelstein, Increased Expression of

the Epidermal Growth Factor Receptor Gene in Malignant Gliomas Is Invariably Associated with Gene Amplification, *Proc. Natl. Acad. Sci. U. S. A.*, 1987, **84**(19), 6899–6903, DOI: 10.1073/pnas.84.19.6899.

4 D. J. Hicklin and L. M. Ellis, Role of the Vascular Endothelial Growth Factor Pathway in Tumor Growth and Angiogenesis, *J. Clin. Oncol.*, 2005, **23**(5), 1011–1027, DOI: 10.1200/JCO.2005.06.081.

5 M. Malumbres and M. Barbacid, Cell Cycle, CDKs and Cancer: A Changing Paradigm, *Nat. Rev. Cancer*, 2009, **9**(3), 153–166, DOI: 10.1038/nrc2602.

6 J. D. Benson, Y.-N. P. Chen, S. A. Cornell-Kennon, M. Dorsch, S. Kim, M. Leszczyniecka, W. R. Sellers and C. Lengauer, Validating Cancer Drug Targets, *Nature*, 2006, **441**, 451–456, DOI: 10.1038/nature04873.

7 J. Downward, Targeting RAS Signalling Pathways in Cancer Therapy, *Nat. Rev. Cancer*, 2003, **3**(1), 11–22, DOI: 10.1038/nrc969.

8 R. Roskoski Jr., FDA-approved small molecule protein kinase inhibitorshttps://www.brimr.org/PKI/PKIs.htm (accessed Oct 25, 2021).

9 S. Omura, H. Tanaka, R. Oiwa, J. Awaya, R. Masuma and K. Tanaka, New Antitumor Antibiotics, OS-4742 A1, A2, B1 and B2 Produced by a Strain of Streptomyces, *J. Antibiot.*, 1977, **30**(11), 908–916.

10 L. M. Toledo and N. B. Lydon, Structures of Staurosporine Bound to CDK2 and CAPK - New Tools for Structure-Based Design of Protein Kinase Inhibitors, *Structure*, 1997, **5**(12), 1551–1556, DOI: 10.1016/S0969-2126(97)00304-3.

11 J. Berger, Staurosporine, a Potent Inhibitor of Phospholipid/Ca++ Dependent Protein Kinase, *Biochem. Biophys. Res. Commun.*, 1986, **135**(2), 397–402.

12 G. E. Atilla-Gokcumen, D. S. Williams, H. Bregman, N. Pagano and E. Meggers, Organometallic Compounds with Biological Activity: A Very Selective and Highly Potent Cellular Inhibitor for Glycogen Synthase Kinase 3, *ChemBioChem*, 2006, **7**(9), 1443–1450, DOI: 10.1002/cbic.200600117.

13 J.É Debreczeni, A. N. Bullock, G. E. Atilla, D. S. Williams, H. Bregman, S. Knapp and E. Meggers, Ruthenium Half-Sandwich Complexes Bound to Protein Kinase Pim-1, *Angew. Chem., Int. Ed.*, 2006, **45**(10), 1580–1585, DOI: 10.1002/anie.200503468.

14 R. Anand, J. Maksimoska, N. Pagano, E. Y. Wong, P. A. Gimotty, S. L. Diamond, E. Meggers and R. Marmorstein, Toward the Development of a Potent and Selective Organoruthenium Mammalian Sterile 20 Kinase Inhibitor, *J. Med. Chem.*, 2009, **52**(6), 1602–1611, DOI: 10.1021/jm8005806.

15 H. Bregman and E. Meggers, Ruthenium Half-Sandwich Complexes as Protein Kinase Inhibitors: An N-Succinimidyl Ester for Rapid Derivatizations of the Cyclopentadienyl Moiety, *Org. Lett.*, 2006, **8**(24), 5465–5468, DOI: 10.1021/ol0620646.

16 Y. Zheng and D. Pan, The Hippo Signaling Pathway in Development and Disease, *Dev. Cell*, 2019, **50**(3), 264–282, DOI: 10.1016/j.devcel.2019.06.003.

17 F. Fan, Z. He, L. L. Kong, Q. Chen, Q. Yuan, S. Zhang, J. Ye, H. Liu, X. Sun, J. Geng, L. Yuan, L. Hong, C. Xiao, W. Zhang, X. Sun, Y. Li, P. Wang, L. Huang, X. Wu, Z. Ji, Q. Wu, N. S. Xia, N. S. Gray, L. Chen, C. H. Yun, X. Deng and D. Zhou, Pharmacological Targeting of Kinases MST1 and MST2 Augments Tissue Repair and Regeneration, *Sci. Transl. Med.*, 2016, **8**(352), 1–14, DOI: 10.1126/scitranslmed.aaf2304.

18 M. Scarpi-Luttenauer, K. Galentino, C. Orvain, M. Cecchini, C. Gaiddon and P. Mobian, TiO4N2 Complexes Formed with 1,10-Phenanthroline Ligands Containing a Donor-Acceptor Hydrogen Bond Site: Synthesis, Cytotoxicity and Docking Experiments, *Inorg. Chim. Acta*, 2022, **540**, 121036, DOI: 10.1016/j.ica.2022.121036.

19 S. Arribas, O. F. Wendt, S. Siegel and W. Kenneth, 4,5,9-Triazaphenanthren-10-One. 2005.

20 K. M. Deo, D. L. Ang, B. McGhie, A. Rajamanickam, A. Dhiman, A. Khoury, J. Holland, A. Bjelosevic, B. Pages, C. Gordon and J. R. Aldrich-Wright, Platinum Coordination Compounds with Potent Anticancer Activity, *Coord. Chem. Rev.*, 2018, **375**, 148–163, DOI: 10.1016/j.ccr.2017.11.014.

21 H. Yin, J. Roque, P. Konda, S. Monro, K. L. Colo, S. Gujar, R. P. Thummel, L. Lilge, C. G. Cameron and S. A. Mcfarland, Transition Metal Complexes and Photodynamic Therapy from a Tumor-Centered Approach : Challenges, Opportunities, and Highlights from the Development of TLD1433, *Chem. Rev.*, 2019, **119**(2), 797–828, DOI: 10.1021/acs.chemrev.8b00211.

22 Pragti, B. K. Kundu and S. Mukhopadhyay, Target Based Chemotherapeutic Advancement of Ruthenium Complexes, *Coord. Chem. Rev.*, 2021, **448**, 214169–214209, DOI: 10.1016/j.ccr.2021.214169.

23 Y. Lu, D. Zhu, Q. Le, Y. Wang and W. Wang, Ruthenium-Based Antitumor Drugs and Delivery Systems from Monotherapy to Combination Therapy, *Nanoscale*, 2022, **14**(44), 16339–16375, DOI: 10.1039/d2nr02994d.

24 L. Zeng, P. Gupta, Y. Chen, E. Wang, L. Ji, H. Chao and Z. S. Chen, The Development of Anticancer Ruthenium(II) Complexes: From Single Molecule Compounds to Nanomaterials, *Chem. Soc. Rev.*, 2017, **46**(19), 5771–5804, DOI: 10.1039/c7cs00195a.

25 C. Licona, J. B. Delhorme, G. Riegel, V. Vidimar, R. Cerón-Camacho, B. Boff, A. Venkatasamy, C. Tomasetto, P. Da Silva Figueiredo Celestino Gomes, D. Rognan, J. N. Freund, R. Le Lagadec, M. Pfeffer, I. Gross, G. Mellitzer and C. Gaiddon, Anticancer Activity of Ruthenium and Osmium Cyclometalated Compounds: Identification of ABCB1 and EGFR as Resistance Mechanisms, *Inorg. Chem. Front.*, 2020, **7**(3), 678–688, DOI: 10.1039/c9qi01148j.

26 C. Gaiddon and M. Pfeffer, The Fate of Cycloruthenated Compounds: From C–H Activation to Innovative Anticancer Therapy, *Eur. J. Inorg. Chem.*, 2017, **2017**(12), 1639–1654, DOI: 10.1002/ejic.201601216.

27 S. Ma, Z. Meng, R. Chen and K. L. Guan, The Hippo Pathway: Biology and Pathophysiology, *Annu. Rev. Biochem.*, 2019, **88**, 577–604, DOI: 10.1146/annurev-biochem-013118-111829.

28 E. B. Wright and D. A. Lannigan, Therapeutic Targeting of P90 Ribosomal S6 Kinase, *Front. Cell Dev. Biol.*, 2023, **11**, 1–15, DOI: **10.3389/fcell.2023.1297292**.

29 A. P. Halverson, T. A. Elmaaty and L. W. Castle, Complexes of (Bpy) 2Ru(II) and (Ph 2bpy) 2Ru(II) with a Series of Thienophenanthroline Ligands: Synthesis, Characterization, and Electronic Spectra, *J. Coord. Chem.*, 2011, **64**(21), 3693–3699, DOI: **10.1080/00958972.2011.629296**.

30 R. Le Lagadec, L. Rubio, L. Alexandrova, R. A. Toscano, E. V. Ivanova, R. Meškys, V. Laurinavičius, M. Pfeffer and A. D. Ryabov, Cyclometalated N,N-Dimethylbenzylamine Ruthenium(II) Complexes [Ru(C6HR1R2R3-o-CH2NMe2)(Bpy)(RCN)2]PF6 for Bioapplications: Synthesis, Characterization, Crystal Structures, Redox Properties, and Reactivity toward PQQ-Dependent Glucose Dehydrogenase, *J. Organomet. Chem.*, 2004, **689**(25), 4820–4832, DOI: **10.1016/j.jorganchem.2004.09.056**.

31 B. Boff, M. Ali, L. Alexandrova, N. A. Espinosa-Jalapa, R. O. Saavedra-Díaz, R. Le Lagadec and M. Pfeffer, Rational Synthesis of Heteroleptic Tris(Chelate) Ruthenium Complexes [Ru, *Organometallics*, 2013, **32**(18), 5092–5097, DOI: **10.1021/om400611t**.

32 A. D. Ryabov, V. S. Sukharev, L. Alexandrova, R. Le Lagadec and M. Pfeffer, New Synthesis and New Bio-Application of Cyclometalated Ruthenium(II) Complexes for Fast Mediated Electron Transfer with Peroxidase and Glucose Oxidase, *Inorg. Chem.*, 2001, **40**(25), 6529–6532, DOI: **10.1021/ic010423h**.

33 A. D. Ryabov, R. Le Lagadec, H. Le; Estevez, R. A. Toscano, S. Hernandez, L. Alexandrova, V. S. Kurova, A. Fischer, C. Sirlin and M. Pfeffer, Synthesis, Characterization, and Electrochemistry of Biorelevant Photosensitive Low-Potential Orthometalated Ruthenium Complexes, *Inorg. Chem.*, 2005, **44**(5), 1626–1634, DOI: **10.1021/ic048270w**.

34 N. Queyriaux, E. Giannoudis, J. F. Lefebvre, V. Artero and M. Chavarot-Kerlidou, Synthesis of Ruthenium Tris-Diimine Photosensitizers Substituted by Four Methylphosphonate Anchoring Groups for Dye-Sensitized Photoelectrochemical Cell Applications, *Eur. J. Inorg. Chem.*, 2019, **2019**(15), 2154–2161, DOI: **10.1002/ejic.201900151**.

35 N. S. Ng, P. Leverett, D. E. Hibbs, Q. Yang, J. C. Bulanadi, M. Jie Wu and J. R. Aldrich-Wright, The Antimicrobial Properties of Some Copper(II) and Platinum(II) 1,10-Phenanthroline Complexes, *Dalton Trans.*, 2013, **42**(9), 3196–3209, DOI: **10.1039/c2dt32392c**.

36 B. J. Pages, F. Li, P. Wormell, D. L. Ang, J. K. Clegg, C. J. Kepert, L. K. Spare, S. Danchaiwijit and J. R. Aldrich-Wright, Synthesis and Analysis of the Anticancer Activity of Platinum(II) Complexes Incorporating Dipyridoquinoxaline Variants, *Dalton Trans.*, 2014, **43**(41), 15566–15575, DOI: **10.1039/c4dt02133a**.

37 A. M. Krause-Heuer, R. Grunert, S. Kuhne, M. Buczkowska, N. J. Wheate, D. D. Le Pevelen, L. R. Boag, D. M. Fisher, J. Kasparkova, J. Malina, P. J. Bednarski, V. Brabec and J. R. Aldrich-Wright, Studies of the Mechanism of Action of Platinum(II) Complexes with Potent Cytotoxicity in Human Cancer Cells, *J. Med. Chem.*, 2009, **52**(17), 5474–5484, DOI: **10.1021/jm9007104**.

38 L. Leyva, C. Sirlin, L. Rubio, C. Franco, R. Le Lagadec, J. Spencer, P. Bischoff, C. Gaiddon, J. P. Loeffler and M. Pfeffer, Synthesis of Cycloruthenated Compounds as Potential Anticancer Agents, *Eur. J. Inorg. Chem.*, 2007, (19), 3055–3066, DOI: **10.1002/ejic.200601149**.

39 A. Blanchet, A. Bourgmayer, J. E. Kurtz, G. Mellitzer and C. Gaiddon, Isoforms of the P53 Family and Gastric Cancer: A Ménage à Trois for an Unfinished Affair, *Cancers*, 2021, **13**(4), 1–45, DOI: **10.3390/cancers13040916**.

40 L. Depotte, J. Palle, C. Rasola, C. Broudin, V.-A. Afrăsânie, A. Mariani and A. Zaanan, New Developments and Standard of Care in the Management of Advanced Gastric Cancer, *Clin. Res. Hepatol. Gastroenterol.*, 2024, **48**(1), 102245, DOI: **10.1016/j.clinre.2023.102245**.

41 C. Gaiddon, I. Gross, X. Meng, M. Sidhoum, G. Mellitzer, B. Romain, J.-B. Delhorme, A. Venkatasamy, A. C. Jung and M. Pfeffer, Bypassing the Resistance Mechanisms of the Tumor Ecosystem by Targeting the Endoplasmic Reticulum Stress Pathway Using Ruthenium- and Osmium-Based Organometallic Compounds: An Exciting Long-Term Collaboration with Dr. Michel Pfeffer, *Molecules*, 2021, **26**(17), 5386, DOI: **10.3390/molecules26175386**.

42 N. J. Wheate, R. I. Taleb, A. M. Krause-Heuer, R. L. Cook, S. Wang, V. J. Higgins and J. R. Aldrich-Wright, Novel Platinum(II)-Based Anticancer Complexes and Molecular Hosts as Their Drug Delivery Vehicles, *Dalton Trans.*, 2007, (43), 5055–5064, DOI: **10.1039/b704973k**.

43 H. B. J. Jefferies, S. Fumagalli, P. B. Dennis, C. Reinhard, R. B. Pearson and G. Thomas, Rapamycin Suppresses 5′ TOP MRNA Translation through Inhibition of P70(S6k), *EMBO J.*, 1997, **16**(12), 3693–3704, DOI: **10.1093/emboj/16.12.3693**.

44 C. Selman, J. M. A. Tullet, D. Wieser, E. Irvine, S. J. Lingard, A. I. Choudhury, M. Claret, H. Al-qassab, D. Carmignac, A. Woods, I. C. A. Robinson, E. Schuster, R. L. Batterham, L. Partridge, D. Gems and D. J. Withers, Ribosomal Protein S6 Kinase 1 Signaling Regulates Mammalian Lifespan, *Science*, 2009, **326**(5949), 140–144, DOI: **10.1126/science.1177221. Ribosomal**.

45 S. H. Um, F. Frigerio, M. Watanabe, F. Picard, M. Joaquin, M. Sticker, S. Fumagalli, P. R. Allegrini, S. C. Kozma, J. Auwerx and G. Thomas, Absence of S6K1 Protects against Age- and Diet-Induced Obesity While Enhancing Insulin Sensitivity, *Nature*, 2004, **431**(7005), 200–205, DOI: **10.1038/nature02866**.

46 M. Bärlund, F. Forozan, J. Kononen, L. Bubendorf, Y. Chen, M. L. Bittner, J. Torhorst, P. Haas, C. Bucher, G. Sauter and O. Kallioniemi, Detecting Activation of Ribosomal Protein S6 Kinase by Complementary DNA and Tissue Microarray Analysis, *J. Natl. Cancer Inst.*, 2000, **92**(15), 1252–1259.

47 O. Korb, T. Stützle and T. E. Exner, An Ant Colony Optimization Approach to Flexible Protein–Ligand Docking, *Swarm Intell.*, 2007, **1**(2), 115–134, DOI: **10.1007/s11721-007-0006-9**.

48 J. Qin, R. Rajaratnam, L. Feng, J. Salami, J. S. Barber-Rotenberg, J. Domsic, P. Reyes-Uribe, H. Liu, W. Dang, S. L. Berger, J. Villanueva, E. Meggers and R. Marmorstein, Development of Organometallic S6K1 Inhibitors, *J. Med. Chem.*, 2015, **58**(1), 305–314, DOI: **10.1021/jm5011868**.

49 M. F. Adasme, K. L. Linnemann, S. N. Bolz, F. Kaiser, S. Salentin, V. J. Haupt and M. Schroeder, PLIP 2021: Expanding the Scope of the Protein-Ligand Interaction Profiler to DNA and RNA, *Nucleic Acids Res.*, 2021, **49**(W1), W530–W534, DOI: **10.1093/nar/gkab294**.

50 M. Mihmanli, E. Ilhan, U. O. Idiz, A. Alemdar and U. Demir, Recent Developments and Innovations in Gastric Cancer, *World J. Gastroenterol.*, 2016, **22**(17), 4307–4320, DOI: **10.3748/wjg.v22.i17.4307**.

51 H. Wong and T. Yau, Targeted Therapy in the Management of Advanced Gastric Cancer: Are We Making Progress in the Era of Personalized Medicine?, *Oncologist*, 2012, **17**(3), 346–358, DOI: **10.1634/theoncologist.2011-0311**.

52 R. J. Kelly, Immunotherapy for Esophageal and Gastric Cancer, *Am. Soc. Clin. Oncol. Educ. B*, 2017, **37**, 292–300, DOI: **10.1200/EDBK_175231**.

53 Z. Zheng, Y. Zheng, M. Zhang, J. Wang, G. Yu and W. Fang, Reciprocal Expression of P-AMPKa and p-S6 Is Strongly Associated with the Prognosis of Gastric Cancer, *Tumor Biol.*, 2016, **37**(4), 4803–4811, DOI: **10.1007/s13277-015-4193-5**.

54 L. Seeneevassen, P. Dubus, C. Gronnier and C. Varon, Hippo in Gastric Cancer: From Signalling to Therapy, *Cancers*, 2022, **14**(9), 2282–2309, DOI: **10.3390/cancers14092282**.

55 S. Yoshida, K. Matsumoto, T. Arao, H. Taniguchi, I. Goto, T. Hanafusa, K. Nishio and Y. Yamada, Gene Amplification of Ribosomal Protein S6 Kinase-1 and -2 in Gastric Cancer, *Anticancer Res.*, 2013, **33**(2), 469–476.

56 Inc., B. A. SADABS. Madison, WI 2001.

57 G. M. Sheldrick, A Short History of SHELX, *Acta Crystallogr., Sect. A:Found. Crystallogr.*, 2008, **64**(1), 112–122, DOI: **10.1107/S0108767307043930**.

58 G. M. Sheldrick, Crystal Structure Refinement with SHELXL, *Acta Crystallogr., Sect. C:Struct. Chem.*, 2015, **71**, 3–8, DOI: **10.1107/S2053229614024218**.

59 Bruker, *SADABS*. Bruker AXS Inc., Madison, Wisconsin, USA, 2001.